REPORT NO.
UCB/SEMM-97/18

STRUCTURAL ENGINEERING
MECHANICS AND MATERIALS

ON THE CHARACTERIZATION OF LOCALIZED SOLUTIONS IN INELASTIC SOLIDS: AN ANALYSIS OF WAVE PROPAGATION IN A SOFTENING BAR

BY

F. ARMERO

DECEMBER 1997

DEPARTMENT OF CIVIL ENGINEERING
UNIVERSITY OF CALIFORNIA
BERKELEY, CALIFORNIA

On the Characterization of Localized Solutions in Inelastic Solids: An Analysis of Wave Propagation in a Softening Bar

by

F. ARMERO

Structural Engineering, Mechanics and Materials
Department of Civil and Environmental Engineering
University of California, Berkeley CA 94720, USA
armero@ce.berkeley.edu

Abstract

This paper presents a study of the solutions characteristic of the localized failures in inelastic solids under general dynamic conditions. The paper is divided in two parts. In the first part, we present a general framework for the inclusion of localized dissipative mechanisms in a local continuum. This is accomplished by the consideration locally of discontinuities in the displacement field, the so-called strong discontinuities, as a tool for the modeling of these localized effects of the material response. We present in this context a thermodynamically based derivation of the resulting governing equations along these discontinuities. These developments are then incorporated in the local continuum framework characteristic of typical large-scale structural systems of interest. The general multi-dimensional case is assumed in this first part of the paper. In the second part, we present in the context furnished by the previous discussion a study of the wave propagation in the one-dimensional case of a localized softening bar. We obtain first the exact closed-form solution involving a strong discontinuity with a general localized softening law. We consider next the approximate problem involving the softening response of the material in a zone of finite length. Closed-form analytic solutions are obtained for the case of a linear softening law. This analysis reveals the properties of the approximation introduced by the spatial discretization in numerical solutions of the problems. Finally, we present finite element simulations that confirm the conclusions drawn from the previous analyses.

1. Introduction

The failure of many engineering materials is often characterized by the localization of the inelastic effects in small zones, usually band-type patterns, previous to the final collapse of the solid or structure. Typical examples are adiabatic shear banding in metals (BAI & DODD [1992]), shear bands in soils (VARDOULAKIS [1978]), and localization bands of cracking in brittle materials like concrete and rocks (READ & HEGEMEIER [1984]), to mention just one representative reference among many others. Given the clear implications for practical applications, the analysis and numerical simulation of this phenomenon have received an important amount of attention.

As the name strain localization implies, localized solutions are characterized by narrow zones where the strain concentrates. Narrowness is understood in terms of much larger characteristic lengths in the particular problem under study. The multiple-scale nature of the problem is then apparent, with the large scale governing the overall response of the solid or structure previous to failure, but with the small-scale effects controlling the characteristic softening response of the solid at failure previous to its final collapse. This multi-scale setting is common to many other problems in solid and fluid mechanics, and as described in HUGHES [1996], its consideration leads to the proper context for the development of numerical methods for their analysis. The interest in this type of formulations is nowadays very intensive, and motivates in part the presentation in this paper.

The high levels of strain present in the narrow localization bands lead to the concentration of the inelastic response of the material and the corresponding energy dissipation in these localized zones. In fact, the appearance of strain localization needs to be understood backwards as a consequence of the inelastic effects in the material. In this way, the inception of localized solutions has been related to a material bifurcation caused by the change of type of the governing equations in rate-independent inelastic solids or, in the general context of rate-dependent models, as the appearance of unstable modes in spectral analyses of the linearized governing equations. Classical references for the former are THOMAS [1961], HILL [1962], and MANDEL [1966], with more recent accounts presented in RICE [1976], OTTOSEN & RUNESSON [1991], and NEILSEN & SCHREYER [1993]. The rate-dependent case can be found treated in detail in MOLINARI & CLIFTON [1987], among many other references.

The multi-scale character of the problem makes the analysis and numerical simulation of these localized solutions difficult. The first difficulty appears when the constitutive model does not have the information regarding the small scales. This is the case for local, rate-independent inelastic models. These models do not define a characteristic length and, therefore, the concept of a band of finite width is lost, leading necessarily to the consideration of the limiting surfaces. An infinite strain in the limit case of a band of zero thickness corresponds to a discontinuous displacement across the limiting surface. The existence of these discontinuous solutions, referred to as strong-discontinuities, has been

shown in rigorous analyses of the boundary value problem of rate-independent plasticity; see JOHNSON [1976], MATTHIES et al [1979], SUQUET [1981], and the complete account in TEMAM [1984]. These solutions are consistent with the change of type of the governing equations from elliptic to hyperbolic in the quasi-static problem, with the discontinuities associated to the real characteristics that appear in the problem. These ideas are not new. In fact, they are found in the early developments of the theory of plasticity (see e.g. PRANDTL [1920]), and are the basis of the classical slip-line theory of rigid plasticity. See e.g. HILL [1950] for complete accounts.

However, the consideration of discontinuous solutions in the displacement field is not enough to arrive to a correct characterization of the phenomenon of strain localization. In this regard, an important contribution was made in BAZANT & BELYTSCHKO [1985], showing clearly this point in the simple one-dimensional setting furnished by the analysis of wave propagation in a softening bar. This problem is studied in detail in the present paper. Briefly, after applying a stress pulse at both ends of a bar, the reflection at the center triggers the activation of the softening response of the material. Assuming a simple one-dimensional inelastic model with continuum strain-softening, BAZANT & BELYTSCHKO [1985] were able to obtain an exact solution of the boundary value problem, which involves a discontinuity in the displacement at the center of the bar. However, since a strain-softening law defines a finite amount of dissipated energy per unit volume, and since the volume of the softening zone is zero, no energy dissipation is associated to the final solution, a completely non-physical result. These inconsistencies have been linked to the ill-posed character of local continuum formulations of rate-independent models with strain-softening and, more importantly, to the lack of a characteristic length in this type of models. We note, however, that the problem can be better characterized by *the absence of a localized dissipative mechanism in classical strain-softening models of the local continuum.*

Different approaches can be found in the literature to overcome these inconsistencies by including a length scale in the constitutive model. We refer to these approaches as *"small-scale regularizations."* A first simple and natural approach is the consideration of rate-dependent models, as investigated in NEEDLEMAN [1988]. However, the small importance of viscous effects in some materials motivated the search for alternative approaches. These alternative formulations include non-local models (BAZANT et al [1984]), higher-order gradient models (COLEMAN & HODGON [1985]), and Cosserat continua (DEBORST & SLUYS [1991]), among many other references. Following with the discussion above, we note the second difficulty in the modeling of strain localization. Even though a particular formulation may include the localized dissipative effects in a band of finite width, the resulting solutions are highly non-smooth as seen in the large-scale limit. In addition, if small length parameters are introduced in the problem, they must be resolved by the tools employed in the analysis (e.g. by the spatial discretization in numerical methods). The issue is not so much of computational cost, but the need of considering alternative (and often complex) formulations when modeling the large-scale response of the solid, even

before localization or away from the localized patterns. These observations identify the main goal of the present work, that is, the formulation and numerical implementation of a general framework that captures the localized dissipative effects while maintaining the structure of the local continuum.

In this context, we presented in SIMO et al [1993] and ARMERO & GARIKIPATI [1996] an analysis of strong discontinuities that showed the consistency of classical rate-independent plasticity models with the presence of a localized softening response along these discontinuities. In particular, we described in ARMERO & GARIKIPATI [1995,96] the formulation of enhanced finite element methods in the general finite deformation range that accommodate at the element level this localized laws. The proposed methods capture the propagation of these discontinuities in an objective and efficient way by maintaining the standard numerical implementation of traditional finite element methods for local continuum models. Related approaches can be found in LARSSON & RUNESSON [1996], OLIVER [1996], and STEINMANN et al [1997] for regularized discontinuities. Similarly, finite element formulations incorporating local enhancements in terms of discontinuous displacement fields have also been presented in ORTIZ et al [1987] and DVORKIN et al. [1990], and in the form of a localization band in BELYTSCHKO et al [1988].

More recently, we have presented in ARMERO [1997] a general framework for the *modeling* of localized dissipative mechanisms in the local continuum. In this way, strong discontinuities are considered as a tool for the modeling of the localized effects observed in the response of the material. We refer to the resulting constitutive models as *localized models.* In this context, we presented in this last reference the so-called *large-scale regularization of regularized models,* viscoplastic models more precisely. As motivated by the discussion presented above, the idea behind this approach is the formulation of a framework that is able to capture the localized dissipation in the large scale, even though the associated small length scales may not be resolved.

The consideration of large-scale models incorporating objectively the localized dissipative effects is not new. In fact, these ideas can be identified as the foundation of the so-called smeared crack approach for the analysis of the cracking in brittle materials; see e.g. BAZANT & OH [1983], WILLAM et al [1984], and ROTS et al [1985], among many others. Similarly, we can include in this group the approaches based on classical constitutive models in combination with a strain-softening modulus regularized through a characteristic length of the spatial discretization employed in the analysis; see e.g. PIETRSZCZAK & MRÓZ [1981] and OLIVER [1989]. However, the formal nature of these regularization approaches motivated much of the interest in the alternative formulations described above. Perhaps, one of the main criticism is the dependence of the constitutive model on artificial length parameters usually related to numerical approximations of the problem, or of unknown origin, but motivated from physical considerations on the energy dissipation required in the final computed solution. One of the goals of the present work is to arrive to a better understanding of these approaches and, at the same time, to develop different

variations and alternatives, like the finite element methods incorporating the propagation of strong discontinuities and the regularization of viscous models mentioned above; see the aforementioned references for details. As discussed herein, these goals are accomplished by focusing in the limit case of the discontinuous solutions of interest, and by developing a systematic procedure for their incorporation in the local continuum.

The paper is divided in two parts. In the first part, we summarize the ideas behind the formulation of localized models, that is, the modeling of localized dissipative mechanisms in the local continuum. After identifying in Section 2.1 the large-scale problem of interest (defined by the classical local formulation of balance of linear momentum), the kinematics of strong discontinuities are summarized briefly in Section 2.2. The crucial aspect of the proposed formulation is the introduction of these discontinuous solutions in a small local neighborhood of a given material point. A complete characterization of the material response in this local neighborhood is then undertaken in Section 2.3. The assumption of a decoupled strain energy function, in term of a bulk and a localized part along the discontinuity, allows for the modeling of the localized dissipative mechanisms of interest. We present briefly the examples of a localized elastoplastic model and a localized anisotropic damage model, both formulated from the principle of maximum inelastic dissipation in a general thermodynamic context.

The incorporation of these local effects into the large-scale problem described previously is presented in Section 2.4. Perhaps the most significant result in these considerations is the identification of the relation equating the dissipation obtained in the local constitutive considerations with the dissipation observed in the large-scale problem as the fundamental equation that allows to arrive to a consistent large-scale formulation incorporating these localized effects objectively. In this way, the resulting model is understood in the limit case of a vanishing local neighborhood. These developments show that the modeling of these localized dissipative mechanisms in the local continuum can be accomplished without the need of introducing smearing or smoothing assumptions of the limit discontinuous solutions. The constructive way in which the proposed procedure is described leads naturally to its finite element implementation. However, this step is not undertaken in this paper; the reader is referred to ARMERO [1997] for further details in this respect.

Instead, the second and main part of the paper reconsiders the one-dimensional problem proposed in BAZANT & BELYTSCHKO [1985] of the wave propagation in a softening bar. A brief description of the problem and of the solution obtained for the case of continuum strain-softening in this last reference is presented in Section 3.1. We obtain next the exact closed-form solution for the limit case of a strong discontinuity incorporating a localized dissipative mechanism, as characterized in the previous discussion. A general cohesive softening law is assumed on the discontinuity. This solution is presented in Section 3.2. The different features of the solution, including the objective energy dissipation and the resulting wave profiles, breaking times, etc. are described in detail and contrasted with the non-physical solution for the strain-softening case.

Next, we consider in Section 4 the same one-dimensional problem but with a finite local neighborhood accounting for the localized softening effects, in the context discussed in Section 2. A linear interpolation of the displacements is assumed in this local neighborhood, thus allowing for the analysis of the effects of typical finite element interpolations in the approximation of the exact limit solution obtained in Section 3. The continuum elastic equation, with no numerical discretization, is maintained in the rest of the bar. This allows to obtain closed-form solutions of the resulting problem and, therefore, characterize in detail the effects of a discrete approximation of the softening response of the material. The extrapolation of the results learned in this analytical study to full finite element simulations is validated in Section 4.2, where we briefly present the results for representative numerical simulations.

Even though our main motivation for considering this approximate problem is, as indicated above, to gain a better understanding of the discretization effects in the approximations of localized solutions, the proposed analysis has other applications. Given the constant stress approximation assumed in the local softening zone, the resulting equations coincide in this simple one-dimensional setting with a classical regularized softening approach, and with the approaches based on a regularized strong discontinuity, as mentioned above. The results presented in this paper apply then to these cases. In fact, the solution obtained herein is an exact closed-form expression for these regularized approaches based on a finite, and fixed, width of the localized zone. Full details are presented in Section 4.1. Finally, we include in Section 5 several conclusions drawn from these analyses.

2. Modeling of Localized Dissipative Mechanisms in Inelastic Solids.

This section summarizes the formulation of localized models, understood as large-scale constitutive models that incorporate a localized dissipative mechanism. By a large-scale model, we refer to a constitutive model formulated in the local continuum framework, as described in Section 1. Localized dissipative effects are modeled independently of the bulk response of the material through the consideration of strong-discontinuities, the limit case. Section 2.3 develops these ideas. Next, the resulting localized dissipative mechanism is incorporated in the original large-scale problem as described in Section 2.4.

For completeness, the developments presented in this section are presented in the general multi-dimensional setting, even though the main interest of the subsequent sections is the analysis of one-dimensional dynamic solutions. Focus is directed to the infinitesimal case.

2.1. Problem definition

Consider a domain $\Omega \subset \mathbb{R}^{n_{\text{dim}}}$ ($n_{\text{dim}} = 1, 2$ or 3) representing the reference placement of a solid body. Given a certain time interval $\bar{T}$, we introduce the displacement field $\boldsymbol{u} : \Omega \times [0, \bar{T}] \to \mathbb{R}^{n_{\text{dim}}}$ and the (symmetric) stress field $\boldsymbol{\sigma} : \Omega \times [0, \bar{T}] \to \mathbb{R}^{n_{\text{dim}} \times n_{\text{dim}}}$. Standard regularity conditions are assumed for the displacement fields $\boldsymbol{u}$, which we refer as the *large-scale displacements*. In particular, the assumed regularity allows for the common consideration of C^0 finite element interpolations. Additional effects due to the localized material response (e.g., discontinuities) are introduced in Section 2.3.

Given this regularity, the weak form of the balance of momentum equations reads then in the standard form

$$\int_\Omega \rho \ddot{\boldsymbol{u}} \cdot \boldsymbol{\eta} \, d\Omega + \int_\Omega \boldsymbol{\sigma} : \boldsymbol{\varepsilon}(\boldsymbol{\eta}) \, d\Omega = \int_\Omega \rho \boldsymbol{b} \cdot \boldsymbol{\eta} \, d\Omega + \int_{\partial_T \Omega} \bar{\boldsymbol{t}} \cdot \boldsymbol{\eta} \, d\Gamma \,, \tag{2.1}$$

for all admissible variations $\boldsymbol{\eta}$, that is, satisfying the homogeneous essential boundary conditions in part of the boundary $\partial_u \Omega \subset \partial\Omega$ where the unknown displacement field $\boldsymbol{u}$ is fixed. In (2.1), we have denoted the specific body force by $\boldsymbol{b} : \Omega \to \mathbb{R}^{n_{\text{dim}}}$ and the applied boundary tractions by $\bar{\boldsymbol{t}} : \partial_T \Omega \to \mathbb{R}^{n_{\text{dim}}}$ acting on the part $\partial_T \Omega \subset \partial\Omega$ of the boundary of the solid, with the usual assumption $\partial_u \Omega \cap \partial_T \Omega = \emptyset$ and $\overline{\partial_u \Omega \cup \partial_T \Omega} = \partial\Omega$ in each of the n_{dim} components. Similarly, we have denoted the acceleration by $\ddot{\boldsymbol{u}} := \partial^2 \boldsymbol{u} / \partial t^2$, the reference density of the solid by ρ, and the infinitesimal *large-scale strain* variations

$$\boldsymbol{\varepsilon}(\boldsymbol{\eta}) := \nabla^s \boldsymbol{\eta} := \tfrac{1}{2} \left[\nabla \boldsymbol{\eta} + (\nabla \boldsymbol{\eta})^T \right] \,, \tag{2.2}$$

where the superscript $(\cdot)^s$ denotes the symmetric part and $(\cdot)^T$ the matrix transpose. Initial conditions $\boldsymbol{u}(\boldsymbol{x}, 0) = \boldsymbol{u}_o(\boldsymbol{x})$ and $\dot{\boldsymbol{u}}(\boldsymbol{x}, 0) = \boldsymbol{v}_o(\boldsymbol{x})$ in the displacements and velocities, respectively, are assumed.

The stress field $\boldsymbol{\sigma}$ is given by the constitutive model developed in the following section. A standard argument based on integration by parts of the weak form (2.1) shows the continuity of tractions, leading to the well-defined vector

$$\boldsymbol{T}_{\Gamma_x} := \boldsymbol{\sigma} \boldsymbol{n} \Big|_{\Gamma_x} \,, \tag{2.3}$$

on a smooth *material surface* Γ_x defining a unit vector $\boldsymbol{n}$ at a point $\boldsymbol{x} \in \Omega$.

2.2. The kinematics of discontinuous solutions

The previous section introduced the large-scale problem leaving undefined the constitutive relation for the stress field. The assumed regularity of the large-scale displacements and corresponding strains may not incorporate all the effects observed in the response of the material. As indicated in Section 1, our goal is the solution of the problem governed

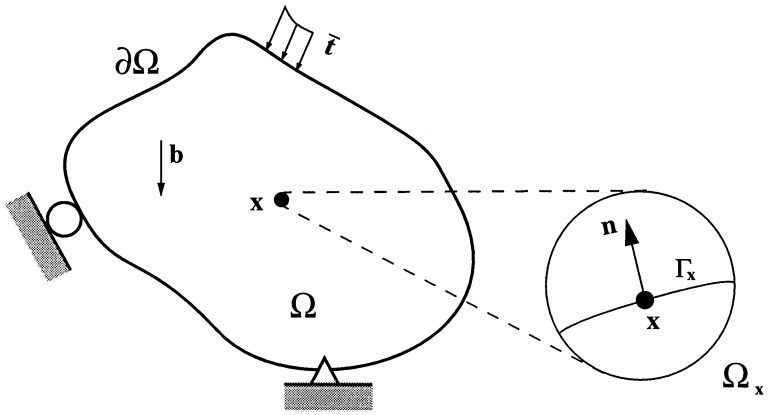

FIGURE 2.1. Illustration of the large-scale problem, involving standard boundary conditions, and the local neighborhood $\Omega_x \subset \Omega$ at a material point $\boldsymbol{x}$, with the smooth surface of displacement discontinuity Γ_x.

by the local equations summarized in the previous section, with the localized effects of the material response taken into account as an added discontinuity of the displacement fields, that is, in the large-scale limit.

To this purpose, consider a local neighborhood $\Omega_x \subset \Omega$ of a material point $\boldsymbol{x} \in \Omega$, whose dimensions and full characterization will be detailed in Section 2.4. In this context, we consider of a discontinuity in the displacement field across a surface $\Gamma_x \subset \Omega_x$ passing through $\boldsymbol{x} \in \Omega_x$ with unit normal $\boldsymbol{n}$. This normal is usually determined by a local condition at $\boldsymbol{x}$, like the loss of ellipticity condition in a elastoplastic solid or the maximum stress direction in a brittle solid; see e.g. ARMERO & GARIKIPATI [1995,96] for details. We then consider the *local* decomposition

$$\boldsymbol{u}_\mu = \boldsymbol{u} + \boldsymbol{\xi}\, M_{\Gamma_x} \qquad \text{in } \Omega_x\ , \tag{2.4}$$

for a smooth function $\boldsymbol{\xi} : \Omega_x \times [0, \bar{T}] \to \mathbb{R}^{n_{\text{dim}}}$, and a function $M_{\Gamma_x} : \Omega_x \to \mathbb{R}$ smooth in $\Omega_x \backslash \Gamma_x$ and normalized to have a unit jump across the discontinuity Γ_x (that is, $[\![M_{\Gamma_x}]\!] = 1$ on Γ_x). If H_{Γ_x} denotes the Heaviside function across Γ_x, the function M_{Γ_x} can be written

$$M_{\Gamma_x} = H_{\Gamma_x} + N_x\ , \tag{2.5}$$

for some smooth function N_x in Ω_x. With these considerations the displacement jump across Γ_x is given by $[\![\boldsymbol{u}_\mu]\!] = \boldsymbol{\xi}$. We note that no compatibility requirements between the large-scale $\boldsymbol{u}$ and small-scale $\boldsymbol{u}_\mu$ displacement fields are imposed a-priori on the local decomposition (2.4).

The infinitesimal strains corresponding to the displacement (2.4) are then given by

$$\boldsymbol{\varepsilon}_\mu = \boldsymbol{\varepsilon}(\boldsymbol{u}) + \boldsymbol{\varepsilon}_{unres} \qquad \text{in} \quad \Omega_x \ , \tag{2.6}$$

where the *unresolved strains* are given by

$$\boldsymbol{\varepsilon}_{unres} = \underbrace{(\boldsymbol{\xi} \otimes \nabla N_{\Gamma_x})^s + \nabla^s \boldsymbol{\xi}\ H_{\Gamma_x}}_{:= \boldsymbol{G}(\boldsymbol{\xi})} + (\boldsymbol{\xi} \otimes \boldsymbol{n})^s\ \delta_{\Gamma_x} \ , \qquad \text{in} \quad \Omega_x \ . \tag{2.7}$$

The singular part of the strain $\boldsymbol{\varepsilon}_\mu$ is expressed in terms of the singular distribution δ_{Γ_x}, the Dirac delta across Γ_x; see STAKGOLD [1979] for mathematical details. The regular part $\bar{\boldsymbol{\varepsilon}}_\mu$ of $\boldsymbol{\varepsilon}_\mu$ can then be written as

$$\bar{\boldsymbol{\varepsilon}}_\mu = \boldsymbol{\varepsilon}(\boldsymbol{u}) + \boldsymbol{G}(\boldsymbol{\xi}) \ , \tag{2.8}$$

for the linear operator $\boldsymbol{G}(\cdot)$ of the displacement jumps $\boldsymbol{\xi}$.

2.3. The localized constitutive model

The previous section summarized the kinematics of strong discontinuities, our tool for the modeling of localized dissipative mechanisms. To characterize a localized dissipative mechanism along Γ_x in the local neighborhood Ω_x, we introduce the following constitutive decomposition of the stored energy in Ω_x

$$W(\boldsymbol{\varepsilon}_\mu, \mathcal{I}) = \bar{W}(\bar{\boldsymbol{\varepsilon}}_\mu, \bar{\mathcal{I}}) + \tilde{W}(\boldsymbol{\xi}, \tilde{\mathcal{I}})\ \delta_{\Gamma_x} \ , \tag{2.9}$$

for a given set of internal variables $\mathcal{I}$. That is, we assume that the stored energy function of the material can be decomposed in a regular part $\bar{W}$ in $\Omega_x \backslash \Gamma_x$ and a singular part $\tilde{W}$ on Γ_x, depending respectively on the regular and singular parts of the small-scale strains and internal variables. Uncoupled thermal conditions are assumed for simplicity. The internal variables $\bar{\mathcal{I}}$ characterize a bulk inelastic response in Ω_x, whereas its singular counterparts $\tilde{\mathcal{I}}$ do so along the discontinuity Γ_x.

The decomposition (2.9) of the stored energy function together with the decomposition (2.6) of the strains results in the decomposition of the dissipation functional

$$\begin{aligned} \mathcal{D}_\mu :&= \int_{\Omega_x} \left[\boldsymbol{\sigma} : \dot{\boldsymbol{\varepsilon}}_\mu - \dot{W} \right] \, d\Omega_x \\ &= \int_{\Omega_x} \underbrace{\left[\boldsymbol{\sigma} : \dot{\bar{\boldsymbol{\varepsilon}}}_\mu - \dot{\bar{W}} \right]}_{:= \bar{\mathcal{D}}_\mu} \, d\Omega_x + \int_{\Gamma_x} \underbrace{\left[\boldsymbol{T} \cdot \dot{\boldsymbol{\xi}} - \dot{\tilde{W}} \right]}_{:= \tilde{\mathcal{D}}_\mu} \, d\Gamma_x \ , \end{aligned} \tag{2.10}$$

after using the relation

$$\int_{\Omega_x} \boldsymbol{\sigma} : (\boldsymbol{\gamma} \otimes \boldsymbol{n})^s\ \delta_{\Gamma_x}\ d\Omega_x = \int_{\Gamma_x} \boldsymbol{T} \cdot \boldsymbol{\gamma}\ d\Gamma_x \ , \tag{2.11}$$

for all the variations of displacement jumps $\boldsymbol{\gamma}$, defining the vector field $\boldsymbol{T}$ on Γ_x in the small scale Ω_x. A decoupled expression of the dissipation is obtained, accounting for the contributions of the continuum and localized dissipative mechanisms, respectively.

The formulation the constitutive equations of the bulk of the material follows standard arguments based on the dissipation functional $\bar{\mathcal{D}}_\mu$, after the decoupling of the localized dissipative mechanism. We proceed with the characterization of the localized dissipative mechanism with the consideration of two model examples.

i. *Example I: An elastoplastic localized model.* An elastoplastic model of the localized dissipative mechanism on Γ_x can be characterized by the additive decomposition of the displacement jumps

$$\boldsymbol{\xi} = \boldsymbol{\xi}^e + \boldsymbol{\xi}^p \,, \tag{2.12}$$

in elastic and plastic parts, respectively. Furthermore, we assume that the localized strain energy $\tilde{W}$ is a function of the elastic (or reversible) part of the displacement jump

$$\tilde{W} = \tilde{W}(\boldsymbol{\xi}^e, \tilde{\alpha}) \,, \tag{2.13}$$

where we have considered a single scalar variable $\tilde{\alpha}$ to model the evolution of the irreversible processes along Γ_x for simplicity in the exposition that follows, and without loss of generality. Introducing the stored energy (2.13) in the localized dissipation $(2.10)_2$, and following standard arguments known as Coleman's method (that is, imposing $\tilde{\mathcal{D}}_\mu \geq 0$ for all admissible processes; see e.g. TRUESDELL & NOLL [1965]) we obtain the relations

$$\boldsymbol{T} = \frac{\partial \tilde{W}}{\partial \boldsymbol{\xi}^e} \qquad \text{and} \qquad \tilde{\mathcal{D}}_\mu = \boldsymbol{T} \cdot \boldsymbol{\xi}^p + q\dot{\tilde{\alpha}} \geq 0 \,, \tag{2.14}$$

with $q := -\partial \tilde{W}/\partial \tilde{\alpha}$. The localized elastoplastic response can be characterized by n_{surf} yield surfaces $\tilde{\phi}_j = \tilde{\phi}_j(\boldsymbol{T}, q)$ depending on the thermodynamical forces $\boldsymbol{T}$ and q conjugate to the rate of internal variables, as identified by the expression of the localized dissipation (2.14). The maximization of the dissipation functional (2.14) constrained by the yield conditions $\tilde{\phi}_j \leq 0$ leads in the rate-independent case to the plastic evolution equations

$$\dot{\boldsymbol{\xi}}^p = \sum_{i=1}^{n_{surf}} \tilde{\gamma}_j \, \frac{\partial \tilde{\phi}_j}{\partial \boldsymbol{T}} \,, \qquad \dot{\tilde{\alpha}} = \sum_{i=1}^{n_{surf}} \tilde{\gamma}_j \, \frac{\partial \tilde{\phi}_j}{\partial q} \,, \tag{2.15}$$

for (localized) consistency parameters $\tilde{\gamma}_j$ satisfying the Kuhn-Tucker loading/unloading conditions

$$\tilde{\phi}_j \leq 0 \,, \quad \tilde{\gamma}_j \geq 0 \,, \quad \text{and} \quad \tilde{\gamma}_j \tilde{\phi}_j = 0 \,, \tag{2.16}$$

and the consistency conditions

$$\tilde{\gamma}_j \dot{\tilde{\phi}}_j = 0 \,, \tag{2.17}$$

for $j = 1, n_{surf}$. For ductile materials, a simple example is furnished by a rigid-plastic slip relation along the discontinuity characterized by the single slip surface

$$\tilde{\phi}(\boldsymbol{T}, \tilde{\alpha}) = \|\boldsymbol{T}_T\| - T_y(\tilde{\alpha}) \leq 0 \ , \tag{2.18}$$

for the tangential component of the traction $\boldsymbol{T}_T$, and $\boldsymbol{\xi}^e \equiv 0$ (i.e., $\tilde{W} = \tilde{W}(\tilde{\alpha})$).

ii. *Example II: A localized anisotropic damage model.* The damaged response of brittle materials due to cracking can be easily considered in this framework by the introduction of the crack compliance $\tilde{\boldsymbol{D}}$ defined by the relation

$$\boldsymbol{\xi} = \tilde{\boldsymbol{D}}\boldsymbol{T} \ . \tag{2.19}$$

The consideration of the localized complimentary energy function

$$\tilde{\chi}(\boldsymbol{T}, \tilde{\boldsymbol{D}}, \tilde{\alpha}) := \boldsymbol{T} \cdot \boldsymbol{\xi} - \tilde{W}(\boldsymbol{\xi}, \tilde{\boldsymbol{D}}, \tilde{\alpha}) = \tfrac{1}{2}\boldsymbol{T} \cdot \tilde{\boldsymbol{D}}\boldsymbol{T} - \tilde{\psi}(\tilde{\alpha}) \ , \tag{2.20}$$

in terms of the internal variables $\tilde{\boldsymbol{D}}$ and $\tilde{\alpha}$, leads to the localized damage dissipation

$$\tilde{\mathcal{D}}_\mu = \tfrac{1}{2}\dot{\tilde{\boldsymbol{D}}} : \boldsymbol{T} \otimes \boldsymbol{T} + q\dot{\tilde{\alpha}} \ , \tag{2.21}$$

The introduction of damage surfaces $\tilde{\phi}_j(\boldsymbol{T} \otimes \boldsymbol{T}, q) \leq 0$ for $j = 1, n_{surf}$, leads after maximization of (2.21) to the localized damage evolution equations

$$\dot{\tilde{\boldsymbol{D}}} = \sum_{j=1}^{n_{surf}} 2\gamma_j \frac{\partial \tilde{\phi}_j}{\partial(\boldsymbol{T} \otimes \boldsymbol{T})} \qquad \text{and} \qquad \dot{\tilde{\alpha}} = \sum_{j=1}^{n_{surf}} \gamma_j \frac{\partial \tilde{\phi}_j}{\partial q} \ , \tag{2.22}$$

with the consistency parameters satisfying the Kuhn-Tucker loading/unloading conditions (2.16) and the consistency conditions (2.17).

Remarks 2.1.

1. Several extensions of the previous developments are readily available. For instance, a Perzyna-type viscous regularization is obtained by replacing the Kuhn-Tucker loading/unloading conditions (2.16) and the consistency relation (2.17) by the evolution equation

$$\dot{\tilde{\gamma}}_j = < \tilde{\phi}_j > / \eta_L \qquad (j = 1, n_{surf}) \ , \tag{2.23}$$

for a localized viscous parameter η_L, and Macaulay brackets $< x >:= (x + |x|)/2$ while retaining the evolution equations (2.15).

2. Similarly, the above developments extend to the finite deformation case with the consideration of the deformation gradient $\boldsymbol{F}_\mu := \text{Grad}\boldsymbol{\varphi}_\mu$ decomposed as in (2.6)

$$\boldsymbol{F}_\mu = \underbrace{\text{Grad}\boldsymbol{\varphi} + \bar{\boldsymbol{F}}_{unres}}_{:=\bar{\boldsymbol{F}}} + [\![\boldsymbol{\varphi}_\mu]\!] \otimes \boldsymbol{N} \ \delta_{\Gamma_x}$$

for a smooth deformation $\boldsymbol{\varphi} : \Omega \times [0, \bar{T}] \to \mathbb{R}^{n_{\text{dim}}}$ and unit material normal $\boldsymbol{N}$. Objective constitutive equations are then developed in terms of the convected components of the material displacement jumps $\boldsymbol{\xi} := \bar{\boldsymbol{F}}^{-1}[\![\boldsymbol{\varphi}_\mu]\!]$ following the same arguments of the infinitesimal case. The reader is referred to ARMERO [1997] for details, including its use in the analysis of strain-localization in rate-dependent solids. □

2.4. The incorporation of the localized dissipation in the local continuum

Section 2.1 considered the large-scale problem in terms of the smooth displacements $\boldsymbol{u}$. The stresses $\boldsymbol{\sigma}$ are obtained in terms of these displacements and the local field $\boldsymbol{\xi}$ in the local neighborhood Ω_x through the localized constitutive model introduced in the previous section. The two problems need to be connected. As indicated in Section 1, our final goal is the solution of the large-scale problem incorporating objectively the observed localized dissipation. Since the constitutive model developed in Section 2.3 accounts objectively for the localized dissipation, the "bridge" connecting the two scales can be accomplished by equating the dissipations observed when solving each problem, as shown by the following developments. In this context, one may refer to this connection as the "equi-dissipation bridge".

The dissipation observed in the local neighborhood $\Omega_x \subset \Omega$ solving (2.1) is given by

$$\mathcal{D} = \int_{\Omega_x} \left[\boldsymbol{\sigma} : \boldsymbol{\varepsilon}(\dot{\boldsymbol{u}}) - \dot{W} \right] \, d\Omega_x \, , \tag{2.24}$$

where $\dot{W}$ corresponds again to the change of free energy of the material in Ω_x and $\dot{\boldsymbol{u}}$ is the rate of large-scale displacement $\boldsymbol{u}$. Comparing (2.24) with (2.10), we observe that the difference between the dissipation rates at the two different scales due to the stress $\boldsymbol{\sigma}$ stems from the difference of the stress power measured with the large and small scale strain rates. Given the decomposition (2.6), we have

$$\mathcal{D} = \mathcal{D}_\mu - \int_{\Omega_x} \boldsymbol{\sigma} : \dot{\boldsymbol{\varepsilon}}_{unres} \, d\Omega_x \, . \tag{2.25}$$

Equating the two dissipation rates for any variation of the local fields leads to the relation

$$\boxed{\int_{\Omega_x} \boldsymbol{\sigma} : \dot{\boldsymbol{\varepsilon}}_{unres} \, d\Omega_x = 0 \, ,} \tag{2.26}$$

for all the variations $\dot{\boldsymbol{\varepsilon}}_{unres}$ of the local unresolved strains. It is important to point out that, if we understand the unresolved strains as the strains enhancing the large-scale strains $\boldsymbol{\varepsilon}(\boldsymbol{u})$, we recover *the orthogonality of the stress and the enhanced strain fields common to enhanced strain finite element formulations* (see SIMO & RIFAI [1990]).

Given the expression (2.7) of the unresolved strains, we conclude that

$$\boldsymbol{r}_{\Omega_x}(\boldsymbol{u},\boldsymbol{\xi};\boldsymbol{\gamma}) := \int_{\Omega_x} \boldsymbol{\sigma}(\boldsymbol{u},\boldsymbol{\xi}) : \boldsymbol{G}(\boldsymbol{\gamma})\, d\Omega_x + \int_{\Gamma_x} \boldsymbol{T}(\boldsymbol{\xi})\cdot\boldsymbol{\gamma}\, d\Gamma_x = 0\ . \tag{2.27}$$

for all variations $\boldsymbol{\gamma}$ of the local field $\boldsymbol{\xi}$. The term $\boldsymbol{T}(\boldsymbol{\xi})$ in (2.27) is given by the localized constitutive model developed in Section 2.3. Equation (2.27) is to be added to the balance of linear momentum equation (2.1) defining the the large-scale problem and the localized model formulated in Section 2.1. It remains to be shown that the final set of equations determines a well-defined formulation in the sense that a solution for the unknown fields (i.e., the large-scale displacement $\boldsymbol{u}$ and the local fields $\boldsymbol{\xi}$) can be found. We show next that this is the case through a limiting procedure that recovers the local continuum framework, defining in the process the operator $\boldsymbol{G}(\boldsymbol{\xi})$.

2.4.1. The consistency with the local continuum framework

An arbitrary fixed neighborhood Ω_x has been assumed in the preceding developments. The model developed to this point exhibits then a non-local structure due to the appearance of this finite neighborhood defining the material response at the point $\boldsymbol{x} \in \Omega$. However, and as indicated in Section 1, our goal is to formulate a constitutive model that recovers *in the limit* the local continuum framework (a *simple material* in the classical terminology introduced in TRUESDELL & NOLL [1965]), and still captures the localized dissipation as described in Section 2.3. The next step is then the consideration of the limit as the measure of Ω_x tends to zero.

To this end, we introduce the following notation

$$A_x := measure(\Omega_x) = \int_{\Omega_x} d\Omega_x\ , \quad l_x := measure(\Gamma_x) = \int_{\Gamma_x} d\Gamma_x\ , \quad \text{and} \quad h_x := \frac{A_x}{l_x}\ , \tag{2.28}$$

The case of interest corresponds to $h_x \to 0$, with $A_x = O({h_x}^{n_{\dim}})$ and $l_x = O({h_x}^{(n_{\dim}-1)})$, so the neighborhood Ω_x reduces to the point $\boldsymbol{x}$ in the limit. The length scale h_x is chosen as the controlling parameter in this limit process.

In this context, we consider the expansions*

$$\boldsymbol{\sigma}(\boldsymbol{y}) = \boldsymbol{\sigma}_x + O(h_x)\ , \quad \boldsymbol{\gamma}(\boldsymbol{y}) = \boldsymbol{\gamma}_x + O(h_x) \qquad \forall \boldsymbol{y} \in \Omega_x\ , \tag{2.29}$$

and

$$\boldsymbol{T}(\boldsymbol{y}) = \boldsymbol{T}_x + O(h_x) \qquad \forall \boldsymbol{y} \in \Gamma_x\ , \tag{2.30}$$

* The standard notation for the "big oh" $O(\cdot)$ (that is, $\lim_{h_x \to 0} O({h_x}^k)/{h_x}^k < \infty$) is considered.

where $(\cdot)_x = (\cdot)(\boldsymbol{x})$, that is, the value of the corresponding quantity at the fixed point $\boldsymbol{x} \in \Omega$. Introducing the expansions (2.29) to (2.30) in (2.27), we obtain after some algebraic manipulations the condition

$$\boxed{\boldsymbol{G}(\boldsymbol{\gamma}) := -\frac{1}{h_x}\,(\boldsymbol{\gamma}_x \otimes \boldsymbol{n})^s + O(1) \qquad \text{in} \quad \Omega_x\ ,} \tag{2.31}$$

for the equation (2.27) to be consistent with the local relation (2.3) (i.e., $\boldsymbol{T}_x = \boldsymbol{\sigma}_x \boldsymbol{n}$) of the large-scale problem as $h_x \to 0$. We observe also that given (2.31), equation (2.27) can be written as

$$\boldsymbol{T}(\boldsymbol{\xi}_x) = \frac{1}{A_x}\int_{\Omega_x} \boldsymbol{\sigma}\boldsymbol{n}\ d\Omega_x + O(h_x)\ , \tag{2.32}$$

identifying the tractions $\boldsymbol{T}$ with the average of $\boldsymbol{\sigma}\boldsymbol{n}$ in Ω_x to first order in the limit $h_x \to 0$. Higher order approximations of $\boldsymbol{G}(\cdot)$ can be obtained by equating higher order terms, leading in principle to the consideration of more details of the strain field in the local neighborhood Ω_x.

It remains to be shown that the displacement jump $\boldsymbol{\xi}_x$ is determined by the nonlinear equation (2.27) in terms of the large-scale displacement $\boldsymbol{u}$ as $h_x \to 0$, leading to a well-defined formulation. To this purpose, we introduce the linearization of the localized softening model

$$\Delta \boldsymbol{T} = \tilde{\boldsymbol{C}}\ \Delta \boldsymbol{\xi}_x \tag{2.33}$$

and the acoustic tensor

$$Q_{ik} = C_{ijkl} n_j n_l \qquad (i,k = 1, n_{\text{dim}})\ , \tag{2.34}$$

associated to the constitutive tangent operator $\boldsymbol{C}$ of the bulk response of the material in Ω_x, that is,

$$\Delta \boldsymbol{\sigma} = \boldsymbol{C}\ \Delta \bar{\boldsymbol{\varepsilon}}_\mu\ ,$$

for the direction $\boldsymbol{n}$. The tensor $\boldsymbol{Q}$ is assumed positive definite. For instance, if the only assumed dissipative mechanism is given by the localized inelastic law along Γ_x, elastic response is considered for the regular part in Ω_x leading in the isotropic case to

$$Q_{ik} = \mu\ \delta_{ik} + (\lambda + \mu)\ n_i\ n_k\ , \tag{2.35}$$

for Lamé constants λ and μ, which is positive definite if $\mu > 0$ and $\lambda + 2\mu > 0$.

With the above notation, we consider the linearization of (2.27) with respect to the local field $\boldsymbol{\xi}_x$ to arrive at the expression

$$D_{\boldsymbol{\xi}}(\boldsymbol{r}_{\Omega_x})\Delta\boldsymbol{\xi}_x = \left[\frac{1}{h_x}\boldsymbol{Q} + \tilde{\boldsymbol{C}}\right]\Delta\boldsymbol{\xi}_x + O(h_x)\ . \tag{2.36}$$

Consider the eigenvalue problem

$$\tilde{\boldsymbol{C}}\boldsymbol{\nu} = \omega\, \boldsymbol{Q}\boldsymbol{\nu}\,, \tag{2.37}$$

in the eigenvalues $\omega \in \mathbb{R}$ and eigenvectors $\boldsymbol{\nu} \in \mathbb{R}^{n_{\text{dim}}}$. Then, a solution of (2.27) in the limit of interest $h_x \to 0$ is assured by the implicit function theorem as long as

$$\omega_{min} + \frac{1}{h_x} > 0\,, \tag{2.38}$$

where $\omega_{min} = min\{w_1, \ldots, w_{n_{\text{dim}}}\}$. Condition (2.38) is satisfied for small h_x, under the assumption of finite ω_{min}. We note that conditions similar to (2.38) appear also in typical finite element implementations of smeared type models constraining the size of the finite element. We refer to WILLAM et al [1986] for further details in this respect.

We conclude that the model developed in the previous sections determines the local displacement jump $\boldsymbol{\xi}_x$ in the limit $h_x \to 0$ in terms of the large-scale displacement $\boldsymbol{u}$, as indicated by the nonlinear equation (2.27). After solving this local equation, the large scale problem is completely formulated entirely in terms of the large-scale field $\boldsymbol{u}$, a process referred to as *static condensation,* specially because of its important implications in the actual numerical implementation of these ideas.

In this way, the smooth displacement $\boldsymbol{u}$ can be understood for $h_x > 0$ as *the large-scale regularization of the localized effects modeled through the strong discontinuity in the small scale.* This aspect is not to be confused with the so-called *regularized strong discontinuity approach,* as in LARSSON & RUNESSON [1996]. In the former approach, the strong discontinuity is smoothed out by a band of constant width *in the small scale,* following the terminology employed here. In the current approach, the static condensation of the local parameters does not eliminate the strong-discontinuity from the formulation. It is available in the small scale through the bridge equation (2.27).

In fact, we note that, given (2.32) and the boundness of the tractions, we conclude that

$$\boldsymbol{n} \cdot \boldsymbol{C}\boldsymbol{\varepsilon}(\Delta\boldsymbol{u}) \sim \frac{1}{h_x}\boldsymbol{Q}\Delta\boldsymbol{\xi}_x + O(1) \qquad \text{in} \qquad \Omega_x\,, \tag{2.39}$$

identifying the singularity of the strains in the limit problem $h_x = 0$. Note that as $h_x \to 0$, the neighborhood Ω_x collapses to the material point $\boldsymbol{x}$, with the total strain given only by the large-scale field $\boldsymbol{\varepsilon}(\boldsymbol{u})$ near the discontinuity. Physically, (2.39) states that in the limit $h_x \to 0$, the strain field in the large-scale problem of interest captures the singularity introduced by the strong discontinuity, being of the order $1/h_x$ at a distance h_x from it.

In conclusion, we have shown that equating the dissipation observed in the large and small scale problems leads to a well-defined formulation consistent, in the limit, with the local continuum structure of the large-scale problem of interest. The proposed approach identifies the corresponding weak form of this condition (2.27) as the sufficient connecting equation between the two problems. This approach is to be compared to the strong

imposition of kinematic compatibility between the small and large scale displacement fields on the boundary of the local neighborhood; see HUGHES [1996] for a discussion in a more general setting.

3. An Analysis of Wave Propagation in a Localized Softening Bar: Exact Closed-Form Solution

We apply the developments described in the previous sections to the analysis of wave propagation in a softening bar. Section 3.1 presents a description of the problem, together with a review of the solution for the elastic and continuum strain-softening cases. The exact solution for the limit case of a strong-discontinuity with a general localized softening law is presented in Section 3.2.

3.1. Problem description: the elastic and strain-softening solutions.

Consider an homogeneous bar $\Omega = [-L, L]$ with constant unit cross section and density ρ, initially at rest. A stress $0 < \sigma_o < \sigma_e$, constant in time, is applied at both ends $x = \pm L$, where σ_e denotes the elastic limit of the material. A linear elastic response, characterized by a Young modulus E, is assumed in this range. The weak form (2.1) leads to the usual one-dimensional longitudinal wave equation in the axial displacement $u(x,t)$

$$\frac{\partial^2 u}{\partial t^2} = c^2 \frac{\partial^2 u}{\partial x^2} \qquad \text{with} \qquad c = \sqrt{\frac{E}{\rho}} \,. \tag{3.1}$$

For the case of interest, the solution involves rectangular stress pulses σ_o propagating from both ends at the speed c. Similarly, rectangular strain and velocity pulses propagate at the same speed with values

$$\varepsilon_o = \frac{\sigma_o}{E} \qquad \text{and} \qquad v_o = c\, \varepsilon_o \,, \tag{3.2}$$

respectively. All the developments that follow extend trivially to the case of a shear layer under simple shear conditions by analogy.

The two pulses meet at the center of the bar at a time that we take as $t = 0$, so we can write

$$u(x,0) = \varepsilon_o \, x \,. \tag{3.3}$$

Upon reflection, the stress doubles in the elastic range (for $2\sigma_o \leq \sigma_e$), imposing the condition

$$u(0,t) = 0 \qquad \Longrightarrow \qquad v(0,t) = 0 \qquad \forall t \,, \tag{3.4}$$

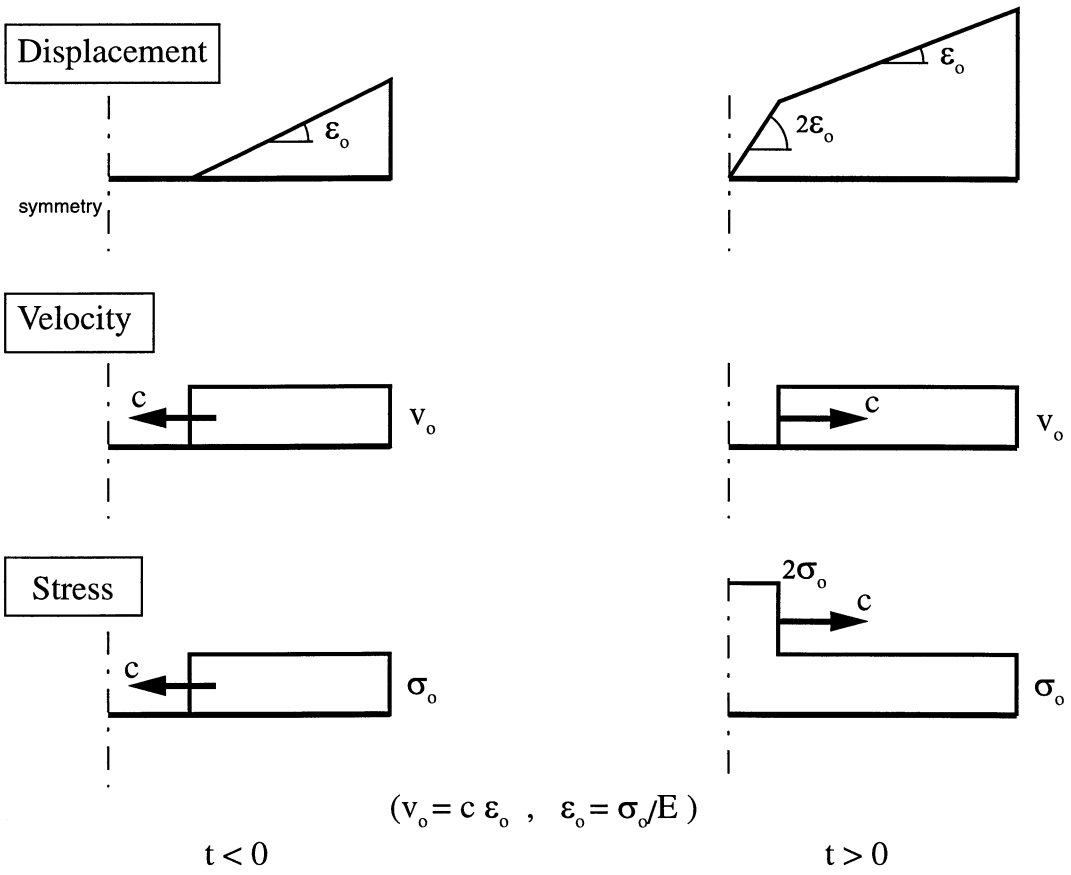

FIGURE 3.1. Wave propagation in a bar. Displacement, velocity and stress distribution for the elastic solution ($2\sigma_o \leq \sigma_e$).

where $v(x,t) = \partial u/\partial t$ denotes the velocity distribution along the bar. Then, loading pulses propagate back at the wave speed c on each side of the bar, with stress value of $2\sigma_o$ and zero velocity. Denoting the one-dimensional Heaviside function by

$$H(\eta) = \begin{cases} 1 & \text{if } \eta > 0, \\ 0 & \text{if } \eta < 0, \end{cases} \tag{3.5}$$

the displacement distribution can be written as

$$u(x,t) = \varepsilon_o\ (x+ct) + \varepsilon_o\ (x-ct)\ H(ct-x) \qquad \text{for } x \geq 0 \quad \text{and} \quad ct \leq L\ . \tag{3.6}$$

Due to the symmetry in the problem, we only consider in the following developments the right half of the bar, that is, $x \geq 0$, with $u(-x,t) = -u(x,t)$ by symmetry. Similarly, since the interest is focused on the wave reflection at the center of the bar, we assume hereafter that $L >> ct$, so no reflection at the opposite ends of the bar needs to be considered. As a consequence, we note the complete equivalence of the assumed problem with the problem defined by imposing the velocity to $\pm v_o$ at $x = \pm L$. This elastic solution is depicted in Figure 3.1. Note again that only half of the bar is depicted due to the symmetry of the solution.

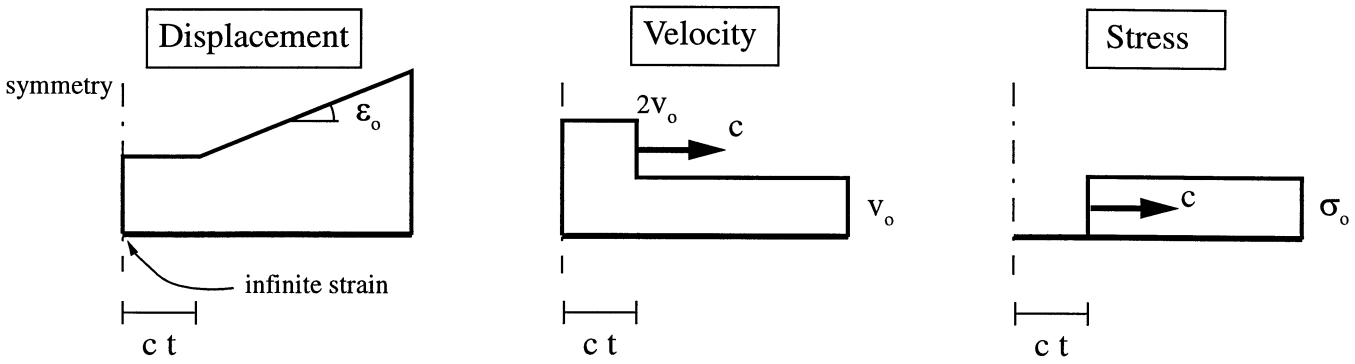

FIGURE 3.2. Wave propagation in a bar. Displacement, velocity and stress distribution for the continuum strain-softening solution ($\sigma_e/2 < \sigma_o \leq \sigma_e$), after BAZANT & BELYTSCHKO [1985].

The solution for the case of a continuum strain-softening bar was obtained by BAZANT & BELYTSCHKO [1985] and is summarized next. Consider an one-dimensional inelastic material model that leads to the stress-strain relation in rate form

$$\dot{\sigma} = K\,\dot{\varepsilon}\,, \qquad \text{with} \quad K = \frac{E\,\mathcal{H}}{E+\mathcal{H}} < 0\,, \tag{3.7}$$

during loading in the inelastic range, characterized initially by the elastic limit σ_e. In (3.7), $\mathcal{H} < 0$ denotes the continuum strain-softening modulus; $E + \mathcal{H} > 0$ is assumed. Introducing the constitutive relation (3.7) in the momentum balance equation (2.1) leads to equation (3.1), but with c^2 replaced by $K/\rho < 0$ in the loading range. A change of type from the original hyperbolic character of (3.1) to elliptic occurs, and the initial boundary value problem becomes ill-posed.

Nevertheless, BAZANT & BELYTSCHKO [1985] observed that a unique solution can still be found having a discontinuous displacement at the center of the bar ($x = 0$), with the associated infinite strain (a Dirac delta function). The solution involves an instantaneous release of the stress at the center of the bar due to the softening response of the material. This leads to an unloading wave that propagates elastically back along the bar. This wave is characterized by a rectangular pulse of zero stress and velocity $2v_0$. The plastic zone is then restricted to the point $x = 0$ only. Figure 3.2 depicts the displacement, velocity and stress distributions corresponding to this solution. Since no unloading from an inelastic state occurs in the process, the solution applies both to a continuum elastoplastic and a continuum damage model characterized by the rate equation (3.7).

This solution is consistent with the idea of the bar breaking at the center upon reflection. Note the zero stress. However, the final energy dissipated in the process vanishes, as a simple calculation shows, indicating the non-physical nature of the solution. BAZANT & BELYTSCHKO [1985] observed that this is due to the fact that the plastic (softening) zone

reduces to a single material point, a consequence to the non-existence of a characteristic length in the constitutive model. Furthermore, the solution does not depend continuously on the data. In fact, the final solution does not depend on the particular form of the softening law.

We can find in the literature several approaches to avoid the above inconsistencies. Many of the proposed regularization approaches involve the introduction of a length scale in the material model, the so-called *localization limiters* as described, for instance, in BAZANT et al [1984]. We refer to these approaches as *"small-scale regularizations,"* and note that the inclusion of any characteristic small length scale in the problem requires its resolution with the tools of analysis available.

In the context of the formulation presented in the previous sections, we observe that the lack of an objective energy dissipation is due to the absence of a localized dissipative mechanism along the strong discontinuity that forms at the center of the bar. We present in the following section the exact analytic solution to the problem incorporating this localized dissipative mechanism in the form of a cohesive softening law at $x = 0$.

3.2. Exact solution for a localized softening model

We obtain next the exact solution under the consideration of a strong discontinuity with a localized dissipative mechanism in the form of a cohesive softening law at $x = 0$. This situation corresponds to the limit case of $h \to 0$ in the discussion of Section 2.4. For the case of a localized rigid-plastic mechanism, we can write the equations

$$\left.\begin{aligned} &\tilde{\phi} = |T| - \tilde{y}(\tilde{\alpha}) \leq 0 \,, \\ &\dot{\xi} = \tilde{\gamma}\ \mathrm{sign}(T) \,, \\ &\dot{\tilde{\alpha}} = \tilde{\gamma} \,, \\ &\tilde{\gamma} \geq 0 \,, \quad \tilde{\gamma}\tilde{\phi} = 0 \,, \quad \tilde{\gamma}\dot{\tilde{\phi}} = 0 \end{aligned}\right\} \tag{3.8}$$

for the displacement jump $\xi(t)$ at $x = 0$. Since no unloading from an inelastic state will occur in the final solution obtained below, the developments below apply to the general elastoplastic response along the discontinuity characterized by equations (2.14) to (2.17) in the general multi-dimensional case. Moreover, under monotonic loading with $T \geq 0$ we also have

$$0 \leq \xi(t) = \tilde{\alpha}(t) \,, \tag{3.9}$$

($\xi = -\tilde{\alpha}$ if $T \leq 0$), as a simple argument based on (3.8) shows.

Remark 3.1. Similarly, the developments below apply also in their entirety to the localized damage model (2.22), since no damaged unloading is involved in the solution.

In this unidimensional setting, the localized constitutive relations (2.22) reduce to the following equations governing the evolution of the crack compliance $\tilde{D}$

$$\left.\begin{aligned} &\xi = \tilde{D}\, T \quad \text{for} \quad T > 0\,, \qquad \xi = 0 \quad \text{for} \quad T \leq 0\,, \\ &\dot{\tilde{D}} = \frac{\tilde{\gamma}}{T}\,, \\ &\dot{\tilde{\alpha}} = \tilde{\gamma}\,, \\ &\tilde{\phi} = T - \tilde{y}(\tilde{\alpha}) \leq 0\,, \\ &\tilde{\gamma} \geq 0\,, \quad \tilde{\gamma}\tilde{\phi} = 0\,, \quad \tilde{\gamma}\dot{\tilde{\phi}} = 0\,, \end{aligned}\right\} \tag{3.10}$$

a model of a brittle bar with tensile strength $\tilde{y}(0) = f'_T$ and cohesive softening law $0 \leq \tilde{y}(\tilde{\alpha}) \leq f'_T$ in the crack. Equation (3.9) applies also to this case. □

We introduce the notation

$$d_o(t) = u(0^+, t) = -u(0^-, t) = \xi(t)/2 \qquad t \geq 0\,, \tag{3.11}$$

for the unknown displacement at the center of the bar $x = 0^+$ (and $x = 0^-$ by symmetry). The rest of the bar remains elastic, with $u(x,t)$ satisfying equation (3.1) for $x > 0$. The solution is then easily obtained as

$$\boxed{u(x,t) = \varepsilon_o\ (x + ct) + \left[\varepsilon_o\ (x - ct) + d_o(t - \frac{x}{c})\right]\ H(ct - x)\,,} \tag{3.12}$$

for $t \geq 0$ and $x > 0$ (symmetric $u(-x,t) = -u(x,t)$ for $x < 0$). Given (3.12), the stress distribution along the bar is given by

$$\sigma(x,t) = \sigma_o + \left[\sigma_o - \frac{E}{c}\ \dot{d}_o(t - \frac{x}{c})\right]\ H(ct - x)\,, \tag{3.13}$$

which particularizes to the value

$$\sigma_{0+}(t) = 2\sigma_o - \frac{E}{c}\ \dot{d}_o(t)\,, \tag{3.14}$$

at $x = 0^+$. After recalling $(3.2)_2$, the velocity distribution is given by

$$v(x,t) = v_o - \left[v_o - \dot{d}_o(t - \frac{x}{c})\right]\ H(ct - x)\,, \tag{3.15}$$

for $t \geq 0$ and $x > 0$ (symmetric $v(-x,t) = -v(x,t)$ for $x < 0$).

The traction $T = T(\xi)$ in (3.8) satisfies equation (2.27) or, equivalently, (2.32). For the current limit case of interest ($h \to 0$), it simply implies the equilibrium relation

$$T = \sigma_{0+}\,. \tag{3.16}$$

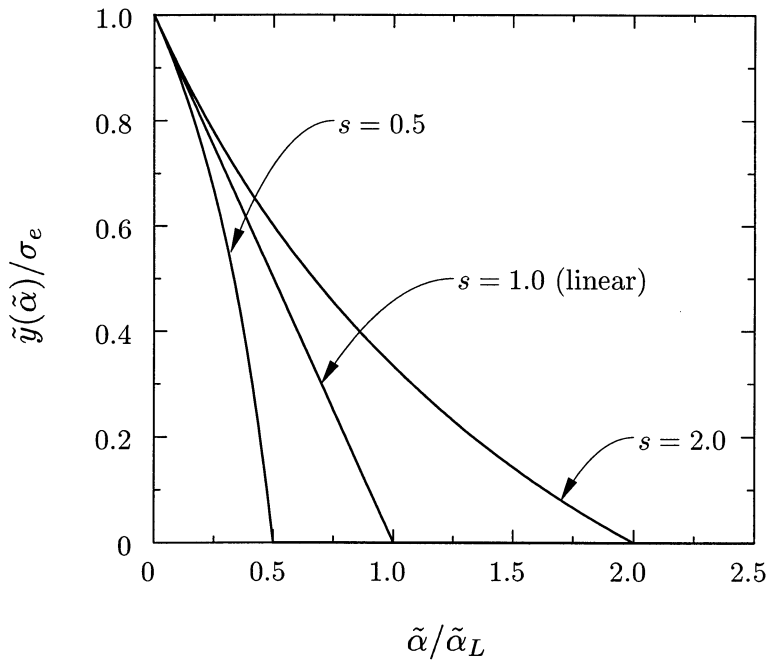

FIGURE 3.3. Localized softening law $\tilde{y}(\tilde{\alpha})$ (3.19) for different values of the non-dimensional parameter $s = \tilde{\alpha}_b/\tilde{\alpha}_L$.

Combining this relation with (3.8) and (3.9), and after noting that $T = \sigma_{0+} \geq 0$, we conclude that

$$\underbrace{\tilde{y}(2d_o(t))}_{T} = \underbrace{2\sigma_o - \frac{E}{c}\,\dot{d}_o(t)}_{\sigma_{0+}}\,, \tag{3.17}$$

a first order ordinary differential equation for $d_o(t)$, with the initial condition $d_o(0) = 0$. The general solution of (3.17) is given by

$$\boxed{2c\,t = \int_0^{2d_o(t)} \frac{E\,d\tilde{\alpha}}{2\sigma_o - \tilde{y}(\tilde{\alpha})}\,,} \tag{3.18}$$

defining implicitly the function $d_o(t)$ in terms of the general localized softening law $\tilde{y}(\tilde{\alpha})$, the incident stress pulse amplitude σ_o, the Young modulus E, and the longitudinal wave speed c of the bar.

As a model example, we consider the general localized softening law

$$\boxed{\tilde{y}(\tilde{\alpha}) = \begin{cases} \sigma_e \left[1 - \dfrac{\tilde{\alpha}}{\tilde{\alpha}_L}\,\dfrac{1}{1 + \dfrac{s-1}{s}\,\dfrac{\tilde{\alpha}}{\tilde{\alpha}_L}}\right}, & \text{for} \quad 0 \leq \tilde{\alpha} \leq \tilde{\alpha}_b = s\,\tilde{\alpha}_L, \\ 0\,, & \text{for} \quad \tilde{\alpha} \geq \tilde{\alpha}_b = s\,\tilde{\alpha}_L, \end{cases}} \tag{3.19}$$

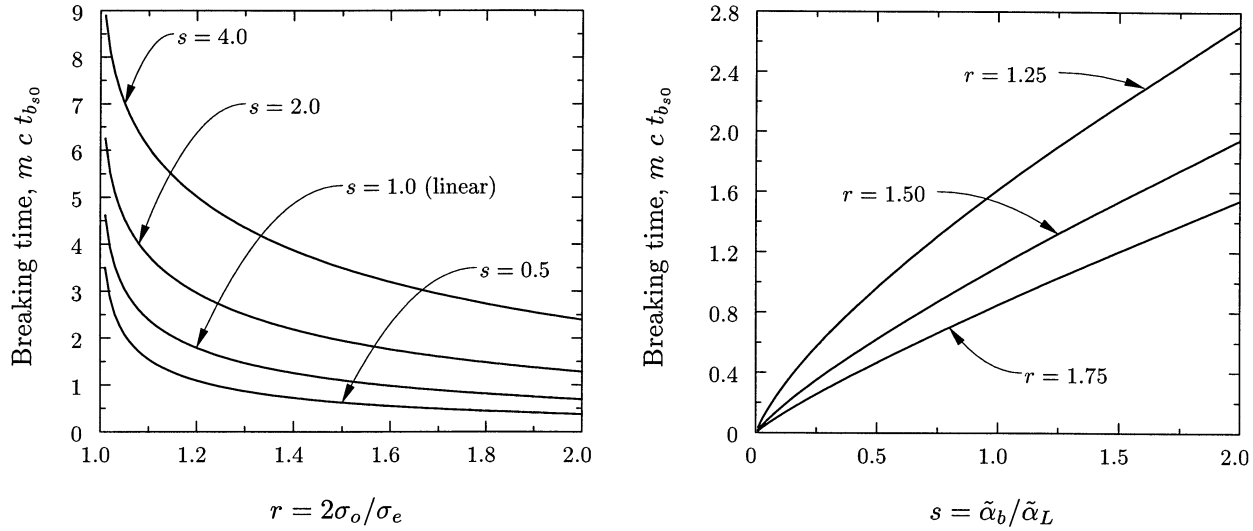

FIGURE 3.4. Non-dimensional breaking time $m\ c\ t_{b_{s0}}$ versus: **a)** $r = 2\sigma_o/\sigma_e$ for $s = \tilde{\alpha}_b/\tilde{\alpha}_L = 0.5$, 1.0 (linear softening), 2.0 and $s = 4.0$. **b)** $s = \tilde{\alpha}_b/\tilde{\alpha}_L$ for $r = 2\sigma_o/\sigma_e = 1.25$, 1.50, and 1.75. Closed-form expression given by equation (3.22).

in terms of the three parameters $\sigma_e > 0$, $\tilde{\alpha}_L > 0$ and $0 < s(= \tilde{\alpha}_L/\tilde{\alpha}_b)$. We note that

$$\tilde{y}(0) = \sigma_e\ , \qquad \tilde{y}(\tilde{\alpha}_b) = 0\ , \qquad \text{and} \qquad \frac{d\tilde{y}}{d\tilde{\alpha}}(0) = -\frac{\sigma_e}{\tilde{\alpha}_L} := \tilde{\mathcal{H}}_L < 0\ , \tag{3.20}$$

which gives an alternative parameter definition in terms of $\tilde{\mathcal{H}}_L$, the initial localized softening modulus. We also observe that a linear softening law is recovered by setting $s = 1$. Figure 3.3 depicts three characteristic examples for different values of the ratio $s = \tilde{\alpha}_b/\tilde{\alpha}_L$.

Defining the "breaking time" $t_{b_{s0}}$ as the time when the stress at the center of the bar vanishes, we have the expression

$$t_{b_{s0}} = \frac{E}{2c}\int_0^{\tilde{\alpha}_b} \frac{d\tilde{\alpha}}{2\sigma_o - \tilde{y}(\tilde{\alpha})}\ , \tag{3.21}$$

after (3.18). The subscript 0 in the symbol for the breaking time is motivated by the introduction in Section 4.1 below of an additional parameter in the analysis. For the general softening model (3.8), the following closed-form expression is obtained after integrating (3.21)

$$\boxed{t_{b_{s0}} = \frac{1}{m\ c\ \beta^2}\left[\log\left(\frac{r\ s}{r-1}\right) + (s-1)\ \beta\right]\ ,} \tag{3.22}$$

where we have introduced the notation

$$m := -\frac{2\tilde{\mathcal{H}}_L}{E} > 0\,, \qquad \beta := r - \frac{1}{s}(r-1) \qquad \text{and} \qquad r := \frac{2\sigma_o}{\sigma_e}\,. \tag{3.23}$$

We observe that m has units of length inverse, whereas r and s are non-dimensional, with

$$1 < r \leq 2\,. \tag{3.24}$$

We also note that

$$d(t_{b_{s0}}) = s\frac{\varepsilon_e}{m} = s\frac{2\varepsilon_o}{mr}\,, \tag{3.25}$$

with $\varepsilon_e := \sigma_e/E$. Relation (3.22) is depicted in Figure 3.4.

Integration of (3.18) for the model defined by (3.19) leads to the implicit expression for $d_o(t)$

$$\boxed{t = \frac{1}{m\,c\,\beta^2}\left[\log\left(1 + \frac{\beta\,r}{r-1}\frac{m\,d_o(t)}{2\varepsilon_o}\right) + \beta\,r\,\frac{s-1}{s}\,\frac{m\,d_o(t)}{2\varepsilon_o}\right]\,, \quad \text{for} \quad 0 \leq t \leq t_{b_{s0}}\,,} \tag{3.26}$$

with

$$\boxed{d_o(t) = s\,\frac{2\varepsilon_o}{m\,r} + 2\,v_o\,(t - t_{b_{s0}})\,, \quad \text{for} \quad t \geq t_{b_{s0}}\,,} \tag{3.27}$$

after recalling (3.2). That is, the bar is released with twice the initial velocity, $2\,v_o$.

For the linear softening case ($s = 1$), equation (3.22) reduces to

$$t_{b_{L0}} = -\frac{1}{m\,c}\,\log\left(1 - \frac{1}{r}\right)\,. \tag{3.28}$$

The subscript L refers to the linear case $s = 1$ hereafter. The solution (3.12) reduces in this case to

$$d_o(t) = \frac{2\varepsilon_o}{m}\,\frac{r-1}{r}\,[\exp(mct) - 1]\,, \qquad \text{for} \quad 0 \leq t \leq t_{b_{L0}}\,, \tag{3.29}$$

and (3.27) for $t \geq t_{b_{L0}}$. The velocity and stress at $x = 0^+$ are then given by

$$\dot{d}_o(t) = 2v_o\,\frac{r-1}{r}\,\exp(mct)\,, \qquad \text{and} \qquad \sigma_{0+} = \sigma_e\,[r - (r-1)\,\exp(mct)]\,, \tag{3.30}$$

for $t \leq t_{b_{L0}}$, and $\dot{d}_o(t) = 2v_o$ and $\sigma_{0+}(t) = 0$ for $t \geq t_{b_{L0}}$.

Defining the energy release rate $\dot{\mathcal{G}}_p$ as the difference between the external power and the total energy stored in the bar (kinetic plus elastic strain energy), we have after integration by parts

$$\tfrac{1}{2}\dot{\mathcal{G}}_p := \sigma_o v_o - \frac{d}{dt}\left[\int_0^L \left[\tfrac{1}{2}v^2 + \tfrac{1}{2}\frac{\sigma^2}{E}\right]\,dx\right] = \tilde{\mathcal{D}}_\mu - \tilde{\psi} = \sigma_{0+}\dot{d}_o(t)\,, \tag{3.31}$$

for the softening potential $\tilde{\psi}$ with $\tilde{y}(\tilde{\alpha}) = \partial\tilde{\psi}/\partial\tilde{\alpha} + \sigma_e$. The 1/2 factor on the left-hand-side of (3.31) accounts for the symmetry in the problem. Combining (3.31) with the solution developed above, we obtain, as expected, the area below the localized softening law, that is,

$$\begin{aligned} \mathcal{G}_p(t) &= \int_0^{2d_o} \tilde{y}(\tilde{\alpha})\, d\tilde{\alpha} \\ &= 2\mathcal{G}_{total_L} \left[\frac{s^2}{(s-1)^2} \log\left(1 + \frac{s}{s-1}\frac{m\, d_o(t)}{\varepsilon_e}\right) - \frac{1}{s-1}\,\frac{m\, d_o(t)}{\varepsilon_e} \right] , \end{aligned} \tag{3.32}$$

for the general softening law (3.8) with $s \neq 1$, and

$$\mathcal{G}_p(t) = 2\mathcal{G}_{total_L}\, \frac{m\, d_o(t)}{\varepsilon_e}\left(1 - \frac{m\, d_o(t)}{2\varepsilon_e}\right) , \tag{3.33}$$

for $s = 1$, where $\mathcal{G}_{total_L} := \sigma_e\varepsilon_e/m$ is the total energy release for the linear softening law. The expression (3.31) is appropriate for the localized rigid-plastic model (3.8) on the discontinuity. For the localized damage model (3.10), the released energy $\mathcal{G}_d$ must be defined

$$\mathcal{G}_d = \mathcal{G}_p - \tfrac{1}{2}\,\tilde{D}\,T^2 , \tag{3.34}$$

accounting for the elastic energy stored on the discontinuity at $x = 0$. A similar term is to be added for a general elastoplastic response on the discontinuity; details are omitted. As expected from physical considerations, the energy released in the solution obtained above is finite.

3.2.1. Properties of the solution

Figure 3.5 depicts the distribution of the displacement ($u\ m/(2\varepsilon_o)$), velocity (v/v_o), and stress (σ/σ_e) along the bar for different times. Figure 3.6 includes the evolution in time of the displacement jump ($\xi\ m/(2\varepsilon_o)$), the velocity ($v(0^+,t)/v_o$), and the stress (σ_{0+}) at $x = 0^+$. The energy release in time is also shown in Figure 3.6 for the localized rigid-plastic model. The softening laws depicted in Figure 3.3 and given by $s = 0.5$, 1, and 2 are considered. In all cases, the value $r = 1.5$ is assumed for the initial stress pulse (i.e., $\sigma_o = 0.75\ \sigma_e$).

The final expressions of the closed-form solution obtained above identify the proper normalizations for the different quantities. With this information, the graphs presented in Figures 3.5 and 3.6 show the proper non-dimensional variables. In particular, the spatial and temporal scales are normalized by the same parameters ($c\ t_{b_{L0}}$ and $t_{b_{L0}}$, respectively), based on the linear softening law $s = 1$, in order to compare the solutions for different softening models. Similarly, the energy release is normalized with the total energy released for the linear case.

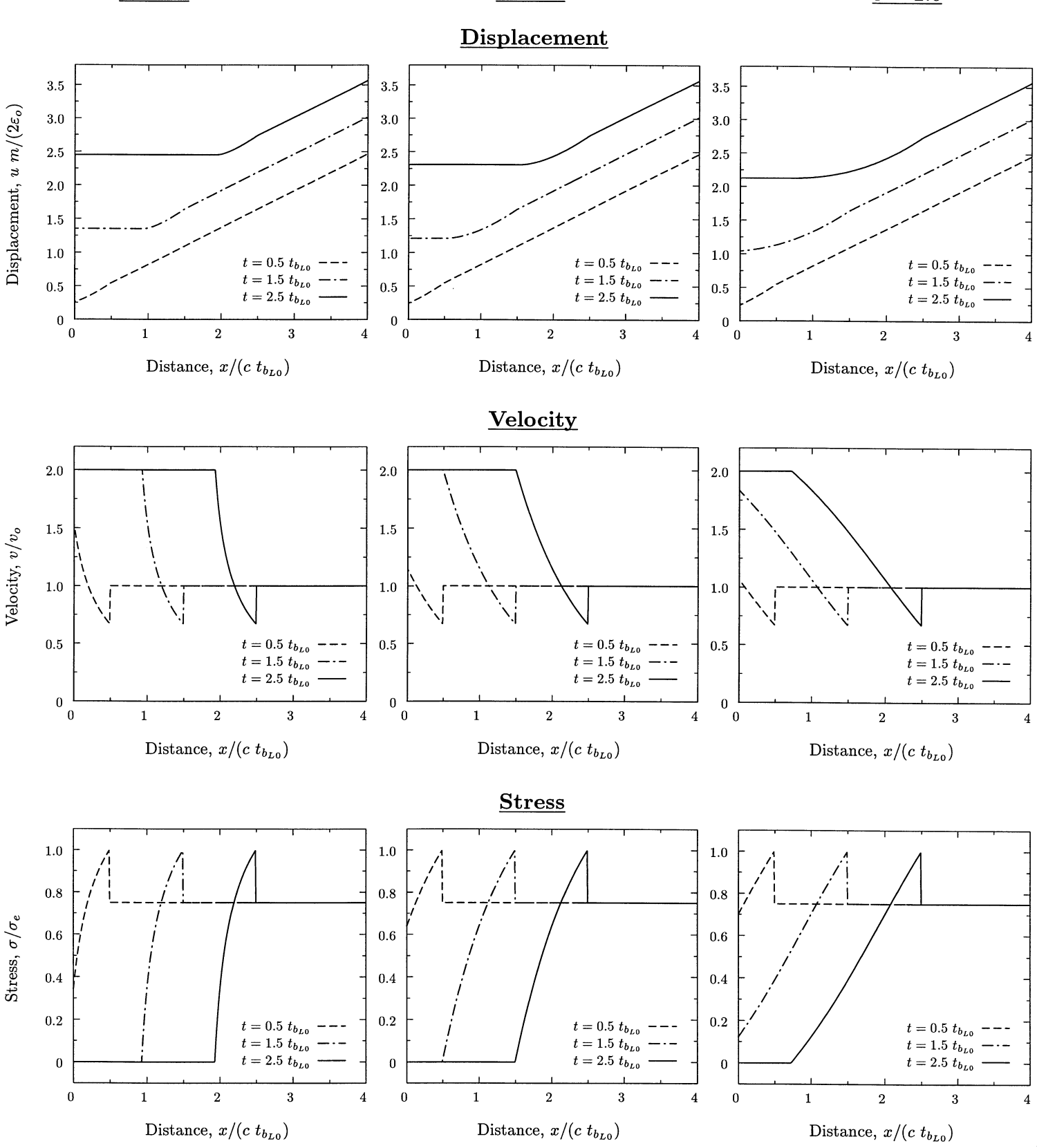

FIGURE 3.5. Displacement, velocity and stress distributions along the bar for different softening laws, $s = 0.5$ (left column), $s = 1.0$ (center column), and $s = 2.0$ (right column), and different times $t/t_{b_{L0}} = 0.5$, 1.5 and 2.5, where $t_{b_{L0}}$ is the breaking time for the linear softening law $s = 1.0$.

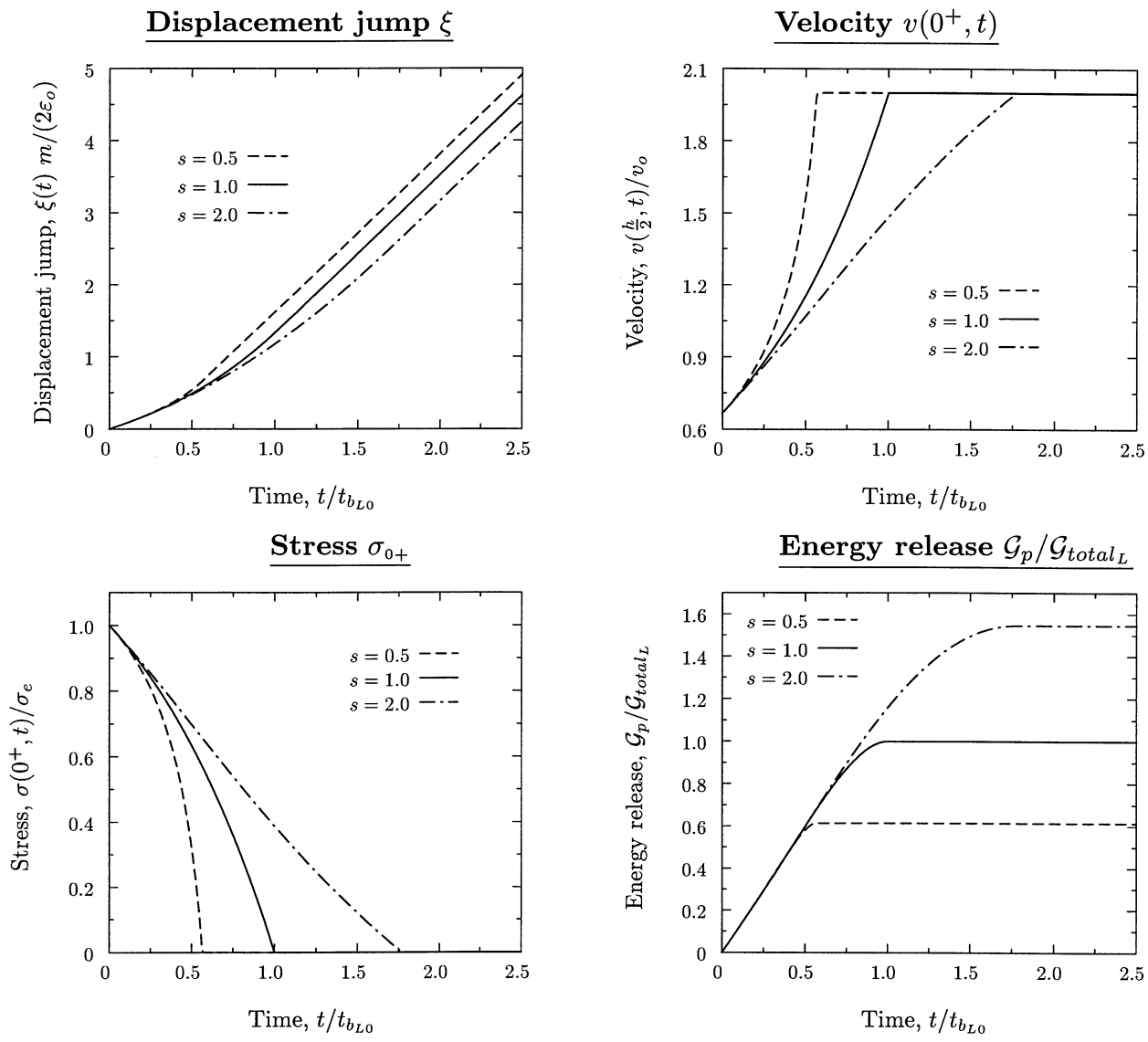

FIGURE 3.6. Displacement jump $\xi(t)$, velocity $v(0^+, t)$, stress σ_{0+}, and energy released $\mathcal{G}_p/\mathcal{G}_{total_L}$ versus time for different softening laws $s = 0.5$, 1.0, and 2.0. The reference value $t_{b_{L0}}$ is the breaking time for the linear case $s = 1$ given by (3.28).

We observe that a loading front of magnitude σ_e in the stress, the elastic limit, forms at $t = 0^+$ upon reflection, instead of doubling ($2\sigma_o > \sigma_e$) as in the elastic solution, or instead of vanishing as in the continuum strain-softening solution. The front propagates back along the bar at the longitudinal wave speed c, with an associated value of the velocity

$$v|_{x=(ct)^-} = c\,(2\varepsilon_o - \varepsilon_e) = 2v_o - c\varepsilon_e\ , \qquad \text{and} \qquad v|_{x=(ct)^+} = v_o\ , \tag{3.35}$$

as it can be easily argued from the balance of linear momentum across the propagating front.

After the sudden formation of this loading front, the localized softening mechanism is activated at $x = 0$. The stress at $x = 0$ is then gradually released from the elastic limit σ_e to zero in a finite time, unloading the bar. The displacement discontinuity at the center of the bar can be easily observed in the plots of the displacement in Figure 3.5. Note again that only the right half of the bar is depicted, and still $u(0^+, t) = d_o(t) \neq 0$. The evolution of this displacement jump is shown also in Figure 3.6. Similarly, the velocity increases in time from the value $(3.35)_1$ to $2v_o$ at the breaking time. We can observe in the time evolutions of Figure 3.6 the increase of the breaking time $t_{b_{s0}}$ with the parameter s, as expected. The dependence of the breaking time on the softening law s is illustrated in Figure 3.4, a plot of relation (3.22). Similarly, the total energy release, the area enclosed by the constitutive relation $\tilde{y}(\tilde{\alpha})$, increases as s increases.

After breaking at $t_{b_{s0}}$, the center of the bar becomes a free end at zero stress. It moves at a constant velocity $2v_o$, twice the initial velocity, for all the cases. The final values of the reflected stress and velocity (0 and $2v_o$, respectively) propagate along the elastic bar at the wave speed c. No further dissipation occurs after breaking.

The differences with the non-physical solution obtained for the continuum strain-softening case depicted in Figure 3.2 are apparent. We observe that one of the main features added by the localized softening mechanism is the introduction of a characteristic time ($t_{b_{s0}}$) during which the dissipation of energy takes place. Given that any signal propagates at the speed c in the elastic bar, this characteristic time defines a profile in the different quantities (stress, velocity and displacement) of width $c\, t_{b_{s0}}$. Using (3.22), we see that this width is given by

$$c\, t_{b_{s0}} = \frac{1}{m\, \beta^2} \left[\log\left(\frac{r\, s}{r-1} \right) + (s-1)\, \beta \right] , \tag{3.36}$$

that is, proportional to the length scale $1/m = -E/(2\tilde{\mathcal{H}}_L)$ defined by the localized softening law. We note that this width depends also on the initial conditions through the parameter r. Therefore, it is not a material property. The presence of the localized dissipative mechanism at $x = 0$ leads in an subtle way to the introduction of dispersive effects in the problem, in the sense that the original rectangular pulses give rise to the aforementioned profile of width $c\, t_{b_{s0}}$. As shown in Figure 3.5, this wave profile is narrower and sharper as s decreases. In fact, we observe that for the limit case $s \to 0$, we recover the solution for the strain-softening continuum model depicted in Figure 3.2, except for the technical point that the stress front at ct is to be understood as the collapse of a front from 0 to σ_e and from σ_e to 0. Note that the limit $s \to 0$ implies no dissipation in the localized dissipative mechanism (a sudden drop of the stress from the elastic limit; see Figure 3.4, and therefore a non-physical response as observed for the continuum solution.

It is important to emphasize that the objective energy dissipation in this exact solution did not require the introduction of a localization limiter, in the sense that no finite

length parameter defining a softening zone is needed. Length scales appear in the solution, as given by (3.36), the width of the resulting propagating wave profiles, but they are not associated to a finite characteristic length of the bar exhibiting a softening response. Instead, we observe that the important feature needed to arrive at an objective solution is simply *the inclusion of the localized dissipative mechanism,* a cohesive softening law along the discontinuity as fully characterized in Section 2 in this local continuum.

Furthermore, the solution that we just found is, apparently, unique. Indeed, we cannot have a solution showing unloading along the discontinuity. For the localized rigid-plastic model (3.8), this would imply $\dot{\xi} = 0$, leading to $\dot{d}_o = 0$ by (3.11). More generally, unloading implies $\dot{\xi} \leq 0$, or equivalently $\dot{d}_o \leq 0$ by (3.11), for the one-dimensional counterparts of the localized elastoplastic model (2.14)-(2.17) or the localized damage model (3.10). But according to (3.14), this would imply a stress higher than the elastic limit σ_e in the bar, and thus it is not a valid solution.

Moreover, we note the continuous dependence of the solution on the constitutive parameters of the material (m, s, and c). In particular, the solution depends continuously on the shape of the localized softening law, as given by the parameter s. This property is to be contrasted with the solution for the ill-posed continuum problem. We also obtain a continuous dependence on the initial conditions in terms of r for $r < 1$ (elastic range) and $1 < r < 2$ (fracture range). At $r = 1$ (that is, $\sigma_o = \sigma_e/2$), the solution changes suddenly from elastic to fracture, a manifestation of the unstable nature of the physical problem (see BAZANT & BELYTSCHKO [1985]).

We conclude this section by pointing out that the exact solution obtained herein does not rely on any smearing or smoothing assumptions. The assumed localized model, understood in the limit described in Section 2.4.1, is mechanically sound, in the sense that no ad-hoc or artificial length parameters are needed to obtain the desired localized energy dissipation. Still, the numerical solution of more complex problems requires the inclusion of these localized effects in a spatially discretized continuum. This motivates the analysis developed in the following section considering a finite softening zone in the context of the formulation presented in Section 2.

4. An Analysis of the Approximation of Strong Discontinuities

We study in this section the effects of a discrete approximation to the exact limit solution obtained in the previous section. In the context described in Section 2, approximate solutions are obtained by considering a finite local neighborhood Ω_x with $h_x > 0$. In fact, the ideas presented in Section 2 apply directly to the development of finite element methods by identifying the local neighborhood $\Omega_x = \Omega_e$, a finite element. These issues can be found discussed in detail in ARMERO [1997].

We consider in Section 4.1 a linear interpolation of the large-scale displacement u in the local neighborhood Ω_x. Our main goal is to clearly identify the effects of the spatial discretization of the softening response. In particular, it is our intention to investigate the approximation properties of common finite element treatments of the problem. However, the proposed analysis provides also the exact closed-form solution for the problem of interest involving the so-called regularized strong discontinuities, where the discontinuity is replaced by a band of finite width. This issue is described in detail in Remark 4.1 below, after the introduction of the governing equations. Finite element simulations of the problem are reported in Section 4.2, confirming the conclusions obtained from the analytical study presented next.

4.1. An approximate solution for $h > 0$: analytical results

The analysis presented in this section is based on the consideration of the following special class of functions approximating the unknown displacement

$$u(x,t) = \begin{cases} d_{\frac{h}{2}}(t)\ \dfrac{2\,x}{h}\ , & \text{for} \quad 0 \le x \le h/2\ , \\ \hat{u}(x,t)\ , & \text{for} \quad x \ge h/2\ , \end{cases} \tag{4.1}$$

for a fixed parameter $h > 0$, with

$$\hat{u}(\frac{h}{2},t) = d_{\frac{h}{2}}(t)\ , \tag{4.2}$$

and symmetric $u(-x,t) = -u(x,t)$ for $x \le 0$. That is, we consider a linear approximation of the displacement $u(x,t)$ in the local neighborhood $\Omega_o = (-h/2, h/2)$ of $x = 0$. This situation is characteristic of linear finite elements (and quadratic elements, in this particular case, by symmetry). A general function $\hat{u}(x,t)$ is assumed outside Ω_o.

We note that the large-scale displacement $u(x,t)$ given by (4.1) is continuous and satisfies the symmetry (boundary) condition $u(0,t) = 0$. As discussed in Section 2, the function $u(x,t)$ is understood as the large-scale regularization of the limit discontinuous solution obtained in Section 3.2. With the assumed class of functions (4.1), the analysis focuses on the effects of a linear approximation of the localized effects of the material characterized by $h > 0$. The effects of a spatial discretization outside the localized zone are neglected. In particular, numerical dispersive effects outside Ω_o are neglected. As shown next, these considerations allow for a complete analytical characterization of the approximate solution. Full finite element simulations are considered separately in Section 4.2.

The particularization of the developments presented in Section 2 to the one-dimensional case of interest leads to the following considerations. The stress σ outside Ω_o is given by the linear elastic relation

$$\sigma = E\ \frac{\partial \hat{u}}{\partial x} \qquad \text{for} \quad x > h/2\ , \tag{4.3}$$

where again we consider only half of the bar by symmetry. The linear approximation of the displacement in Ω_o leads to a constant large-scale strain $\varepsilon(u) = 2\, d_{h/2}/h$. The material response inside the local neighborhood Ω_o is characterized by an elastic response

$$\sigma_{\Omega_o} = E\, \frac{2}{h}\, d_{\frac{h}{2}} \qquad \text{in} \quad \Omega_o\,, \tag{4.4}$$

until the elastic limit σ_e is reached. Thereafter, the material response in Ω_o is characterized by the displacement jump $\xi(t)$ of the small-scale displacements (2.4) at $x = 0$. In the following analysis, we consider the first order approximation of the unresolved strain in the finite local neighborhood Ω_o given by the first term in (2.31), leading to the constant stress

$$\sigma_{\Omega_o} = E\, \left(\frac{2}{h}\, d_{\frac{h}{2}} - \frac{1}{h}\, \xi\right) \qquad \text{in} \quad \Omega_o\,, \tag{4.5}$$

for an elastic response in Ω_o/Γ_o. Given the constant approximation of the unresolved strains and constant stress (4.5) in Ω_o, equation (2.27) leads to the small-scale equilibrium relation

$$T(\xi) = \frac{2}{h} \int_0^{h/2} \sigma\, dx = \sigma_{\Omega_o}\,, \tag{4.6}$$

with $T(\xi)$ given by the localized model at $x = 0$.

We consider again the constitutive relations (3.8) for the localized model along the discontinuity at $x = 0$. Under monotonic loading (as it can be verified a-posteriori), relation (3.9) holds, thus leading to the relation

$$T(\xi) = \tilde{y}(\xi)\,, \tag{4.7}$$

after imposing the consistency condition $\tilde{\phi} = 0$ $(3.8)_1$, and noting also that $T \geq 0$ for the solution obtained below. Similarly, the comments in Remark 3.1 hold, that is, the approximate solution obtained below applies also to the localized damage model (3.10).

Combining (4.7) with (4.5) and (4.6), we obtain during monotonic loading the equation

$$\xi + \frac{h}{E}\, \tilde{y}(\xi) = 2\, d_{\frac{h}{2}}\,, \tag{4.8}$$

defining the displacement jump ξ in terms of $d_{\frac{h}{2}}$. For the general localized softening law (3.19), straightforward algebraic manipulations following the arguments after (2.36) (i.e., imposing that the derivative of the left-hand-side of (4.8) with respect to ξ does not vanish) show that this equation can be solved in ξ if

$$0 \leq \delta := m\, \frac{h}{2} = -\frac{h\, \tilde{\mathcal{H}}_L}{E} < \min\{1, s^2\}\,, \tag{4.9}$$

which is condition (2.38) for the displacement jumps ξ to be uniquely defined in terms of the large-scale displacement $d_{h/2}$ in this particular case. The general solution is obtained by solving a quadratic equation in ξ, and is given by

$$\xi = \frac{\varepsilon_e}{m}\left[\sqrt{R^2 + 4\,B} + R\right] , \tag{4.10}$$

for $s \neq 1$, where

$$R := B - \frac{s}{s-1}(1-\delta) , \qquad B := \frac{m}{\varepsilon_e}\left[d_{\frac{h}{2}} - \delta\frac{\varepsilon_e}{m}\right] , \tag{4.11}$$

and by

$$\xi = \frac{2}{1-\delta}\left[d_{\frac{h}{2}} - \delta\frac{\varepsilon_e}{m}\right] \qquad \text{and} \qquad \sigma_{\Omega_o} = \frac{E\,m}{1-\delta}\left[\frac{\varepsilon_e}{m} - d_{\frac{h}{2}}\right] . \tag{4.12}$$

for the linear softening case $s = 1$. Expressions (4.10) and (4.12) hold before the breaking time $t_{b_{s0}}$, which corresponds to the displacement $d_{\frac{h}{2}}(t_{b_{s0}}) = s\,\varepsilon_e/ms$. After breaking, we have

$$\xi = 2d_{\frac{h}{2}} , \qquad \text{and} \qquad \sigma_{\Omega_o} = 0 , \tag{4.13}$$

during the assumed monotonic loading. Note that for $s = 1$ (linear softening) and in the limit $\delta \to 1$ the bar breaks suddenly (i.e., $\sigma_{\Omega_o} = 0$ as the localized softening law is activated).

Remarks 4.1.

1. We observe that in this one-dimensional case, with linear displacement interpolations and constant approximation of the unresolved strains, the final formulation can be understood as a regularized softening modulus through the length scale h. Note, for example, that the relation $(4.12)_2$ can be written in rate form as

$$\dot{\sigma}_{\Omega_o} = K_h\left(\frac{2}{h}\dot{d}_{\frac{h}{2}}\right) \qquad \text{with} \qquad K_h := -\frac{E\,m}{(1-\delta)}\frac{h}{2} = \frac{E\,(\tilde{\mathcal{H}}_L h)}{E + (\tilde{\mathcal{H}}_L h)} . \tag{4.14}$$

   This expression is characteristic of traditional approaches based on the smearing assumption, with h representing a measure of the finite element size; see e.g. WILLAM et al [1984] or ROTS et al [1985]. The quantity ξ/h can be identified as the "smeared inelastic strain" in this unidimensional setting. For this particular case then, the approach presented in Section 2 focuses on the structure of the limit case of interest ($h \to 0$) underlying the smeared approach, with the variational framework of the resulting localized model described in Section 2.3. The analysis presented below applies then to these more traditional approaches in this case. We note that this analogy does not extend to more general implementations in the multi-dimensional case including, for example, general viscous models in the finite deformation range. We refer to ARMERO [1997] for details.

2. Similarly, the expression (4.14) can be found in constitutive theories that consider a band of finite and constant width (h in the notation above) to represent the localized effects in the material. A constant strain is usually assumed inside the band. We can find in this group the so-called regularized strong discontinuity approach, as in e.g. LARSSON & RUNESSON [1996]. We can also mention the related approach in BELYTSCHKO et al [1988] for similar ideas in the development of finite elements. Therefore, the analysis presented below obtains then the exact closed-form solution for formulations based on this constitutive assumption. We note, however, that the full potential of the general framework presented in Section 2 lies in the objective and systematic modeling of localized dissipative mechanisms in the limit case involving a strong discontinuity, and the proposed framework for the consistent incorporation of the associated singular fields into the local continuum framework of typical large-scale structural problems. The analogy with these approaches does not hold for more general multi-dimensional setting either. □

The introduction of the variations corresponding to the class of functions (4.1) in the weak equation (2.1) leads to

$$\int_0^{\frac{h}{2}} \rho \ddot{d}_{\frac{h}{2}}\, d^*\, \frac{4\,x^2}{h^2}\, dx + \int_0^{\frac{h}{2}} \sigma\, d^*\, \frac{2}{h}\, dx + \int_{\frac{h}{2}}^{L} \rho \ddot{\hat{u}}\, \hat{u}^*\, dx + \int_{\frac{h}{2}}^{L} \sigma\, \frac{\partial \hat{u}^*}{\partial x}\, dx = \hat{u}^*(L,t)\, \sigma_0\,, \tag{4.15}$$

for all variations $\hat{u}^*(x,t)$ with $\hat{u}^*(h/2,t) = d^*(t)$, after making use of the symmetry present in the problem. After integration by parts in $x > h$ and following standard arguments, we arrive at the equations

$$\frac{\partial^2 \hat{u}}{\partial t^2} = c^2\, \frac{\partial^2 \hat{u}}{\partial x^2} \quad \text{for} \quad x > \frac{h}{2}\,, \quad \text{with} \quad \frac{\partial \hat{u}}{\partial x}(L,t) = \varepsilon_o\,, \tag{4.16}$$

and the equation

$$\boxed{\vartheta\, \frac{\rho\, \delta}{m}\, \ddot{d}_{\frac{h}{2}} + \sigma_{\Omega_o} - \sigma_{\frac{h}{2}+} = 0\,,} \tag{4.17}$$

in the unknown function $d_{\frac{h}{2}}(t)$, with $\vartheta = 1/3$ for the consistent mass approximation implied by (4.15) ($\vartheta = 1$ for a lumped mass approximation). Comparing (4.17) and (4.6) with equation (3.16) for the exact limit solution, we observe that the first consequence of the discretization (i.e., $\delta > 0$) is the introduction of an inertial term in the softening response.

The solution of equation (4.16) is given in terms of the unknown function $d_{\frac{h}{2}}(t)$ by

$$\boxed{\hat{u}(x,t) = \varepsilon_o\, (x+ct) + \left[\varepsilon_o\, (x - ct + h) + d_{\frac{h}{2}}(t - \frac{x - h/2}{c})\right]\, H(ct - x + \frac{h}{2})\,,} \tag{4.18}$$

for $ct + h/2 \ll L$ avoiding reflections at $x = L$, as in Section 3.2. Introducing (4.18) in (4.3), we obtain

$$\sigma_{\frac{h}{2}+}(t) = 2\sigma_o - \frac{E}{c}\,\dot{d}_{\frac{h}{2}}(t)\,. \tag{4.19}$$

Therefore, and after using (4.4), the differential equation (4.17) reads

$$\vartheta\frac{\delta}{m\,c}\ddot{d}_{\frac{h}{2}} + \dot{d}_{\frac{h}{2}} + \frac{m\,c}{\delta}d_{\frac{h}{2}} = 2\varepsilon_o \qquad \text{for} \quad t \le t_{e_{L\delta}}\,, \tag{4.20}$$

where $t_{e_{L\delta}}$ denotes the time at which the elastic limit is reached

$$\sigma_{\Omega_o}(t_{e_{L\delta}}) = \sigma_e \qquad \Longleftrightarrow \qquad d_{\frac{h}{2}}(t_{e_{L\delta}}) = \delta\,\frac{\varepsilon_e}{m} = \delta\,\frac{2\varepsilon_o}{m\,r}\,. \tag{4.21}$$

The initial conditions for $d_{\frac{h}{2}}(t)$ are given by (3.3), and read in the notation introduced above as

$$d_{\frac{h}{2}}(0) = \delta\,\frac{\varepsilon_o}{m}\,, \qquad \text{and} \qquad \dot{d}_{\frac{h}{2}}(0) = v_o\,, \tag{4.22}$$

when solving (4.20)

Upon activation of the softening response on the discontinuity $x = 0$ at $t_{e_{L\delta}}$, the differential equation (4.17) reads for the linear softening law $s = 1$

$$\vartheta\frac{\delta}{m\,c}\ddot{d}_{\frac{h}{2}} + \dot{d}_{\frac{h}{2}} - \frac{m\,c}{1-\delta}d_{\frac{h}{2}} = \left(2\varepsilon_o - \frac{1}{1-\delta}\varepsilon_e\right)c \qquad \text{for} \quad t_{e_{L\delta}} \le t \le t_{b_{L\delta}}\,, \tag{4.23}$$

with the breaking time $t_{b_{L\delta}}$ characterized by

$$T(\xi(t_{b_{L\delta}})) = \sigma_{\Omega_o}(t_{b_{L\delta}}) = 0 \qquad \Longleftrightarrow \qquad d_{\frac{h}{2}}(t_{b_{L\delta}}) = \frac{\varepsilon_e}{m} = \frac{2\varepsilon_o}{m\,r}\,. \tag{4.24}$$

After breaking, equation (4.17) reads

$$\vartheta\frac{\delta}{m\,c}\ddot{d}_{\frac{h}{2}} + \dot{d}_{\frac{h}{2}} = 2\varepsilon_o c\,, \qquad \text{for} \quad t \ge t_{b_{L\delta}}\,. \tag{4.25}$$

Continuity of the displacement $d_{\frac{h}{2}}$ and velocity $\dot{d}_{\frac{h}{2}}$ is imposed at $t_{e_{L\delta}}$ and $t_{b_{L\delta}}$.

Equation (4.23) can be easily generalized to the nonlinear softening law $s \neq 1$ using (4.6) and (4.10). The analysis below focuses, however, on the linear softening case $s = 1$, since this assumption allows to obtain closed-form expressions of the final solution. In this way, the linear differential equations (4.20), (4.23) and (4.25) with the initial conditions (4.22) can be solved exactly to arrive at the final expressions

$$d_{\frac{h}{2}}(t) = \delta\frac{2\varepsilon_o}{m} - \delta\,\frac{\varepsilon_o}{m}\left[\cos(\omega_1 t) - \frac{2\vartheta - 1}{\sqrt{4\vartheta - 1}}\,\sin(\omega_1 t)\right]e^{-\gamma t} \qquad \text{for } 0 \le t \le t_{e_{L\delta}}\,, \tag{4.26}$$

$$d_{\frac{h}{2}}(t) = (1-(1-\delta)r)\,\frac{2\varepsilon_o}{m\,r} + \frac{\varepsilon_o}{m}\left[\frac{\gamma}{\omega_2}\left(\frac{\vartheta\delta}{v_o}\dot{d}_{\frac{h}{2}}(t_{e_{L\delta}}) - (1-\delta)\right)\sinh\Big(\omega_2(t-t_{e_{L\delta}})\Big)\right.$$

$$\left. + (1-\delta)\cosh\Big(w_2(t-t_{e_{L\delta}})\Big)\right] e^{-\gamma(t-t_e)} \qquad \text{for } t_{e_{L\delta}} \le t \le t_{b_{L\delta}}\ , \quad (4.27)$$

$$d_{\frac{h}{2}}(t) = \frac{2\varepsilon_o}{m\,r} + \frac{1}{2\gamma}\left[\dot{d}_{\frac{h}{2}}(t_{b_{L\delta}}) - 2v_o\right] e^{-2\gamma(t-t_{b_{L\delta}})} + 2\,v_o\,(t-t_{b_{L\delta}}) \qquad \text{for } t \ge t_{b_{L\delta}}\ , \quad (4.28)$$

where $r = 2\varepsilon_o/\varepsilon_e$ as defined in $(3.23)_3$,

$$\gamma := \frac{mc}{2\vartheta\delta}\ , \qquad \omega_1 := \gamma\sqrt{4\vartheta - 1}\ , \qquad \text{and} \qquad \omega_2 := \gamma\sqrt{1 + 4\frac{\delta}{1-\delta}}\ . \quad (4.29)$$

The times $t_{e_{L\delta}}$ and $t_{b_{L\delta}}$ are found by imposing the values $(4.21)_2$) and $(4.24)_2$ of $d_{\frac{h}{2}}$, respectively.

A simple calculation based on the definition (3.31) shows that the energy release $\mathcal{G}_p$ is given by

$$\dot{\mathcal{G}}_p = 0 \qquad \text{for} \quad t \le t_{e_{L\delta}}\ , \qquad \text{and} \qquad \dot{\mathcal{G}}_p = \sigma_{\Omega_o}\dot{\xi} \qquad \text{for} \quad t_{e_{L\delta}} \le t < t_{b_{L\delta}}\ . \quad (4.30)$$

After integration, the energy release $\mathcal{G}_p$ is given by the same expressions (3.32) and (3.33) for the exact solution with $\delta = 0$, but with d_o replaced by $\xi/2$. The approximate and exact solutions dissipate the same energy for a given value of the displacement jump. The dissipation is then determined only by the localized softening law, *confirming the objectivity of the approximation.* This situation is consistent with the developments of Section 2.4, where the foundation of the regularized formulation with finite Ω_o was identified as the incorporation of this localized energy dissipation in the large-scale problem, the problem solved in this section.

4.1.1. Properties of the solution

Figure 4.1 depicts the distribution of the displacement ($u\ m/(2\varepsilon_o)$), velocity (v/v_o), and stress (σ/σ_e) along the bar at two different times. Figure 3.6 includes the evolution in time of the displacement ($d_{h/2}\ m/(2\varepsilon_o)$) and the velocity ($\dot{d}_{h/2}/v_o$) at $x = h/2$, and the displacement jump ($\xi\ m/(2\varepsilon_o)$) and the stress ($\sigma_{\Omega_o}/\sigma_e$) in Ω_o. The energy release ($\mathcal{G}_p/\mathcal{G}_{total_L}$) for the localized rigid-plastic model is also depicted. Different values of the length parameter δ are considered, in combination with the linear softening law ($s = 1$). In all cases, the value $r = 1.5$ is again assumed for the initial stress pulse (i.e., $\sigma_o = 0.75\ \sigma_e$). A consistent mass approximation ($\vartheta = 1/3$) is assumed; similar results apply to the lumped approximation ($\vartheta = 1$). We have used the same normalization parameters as in the exact solution described in the previous section.

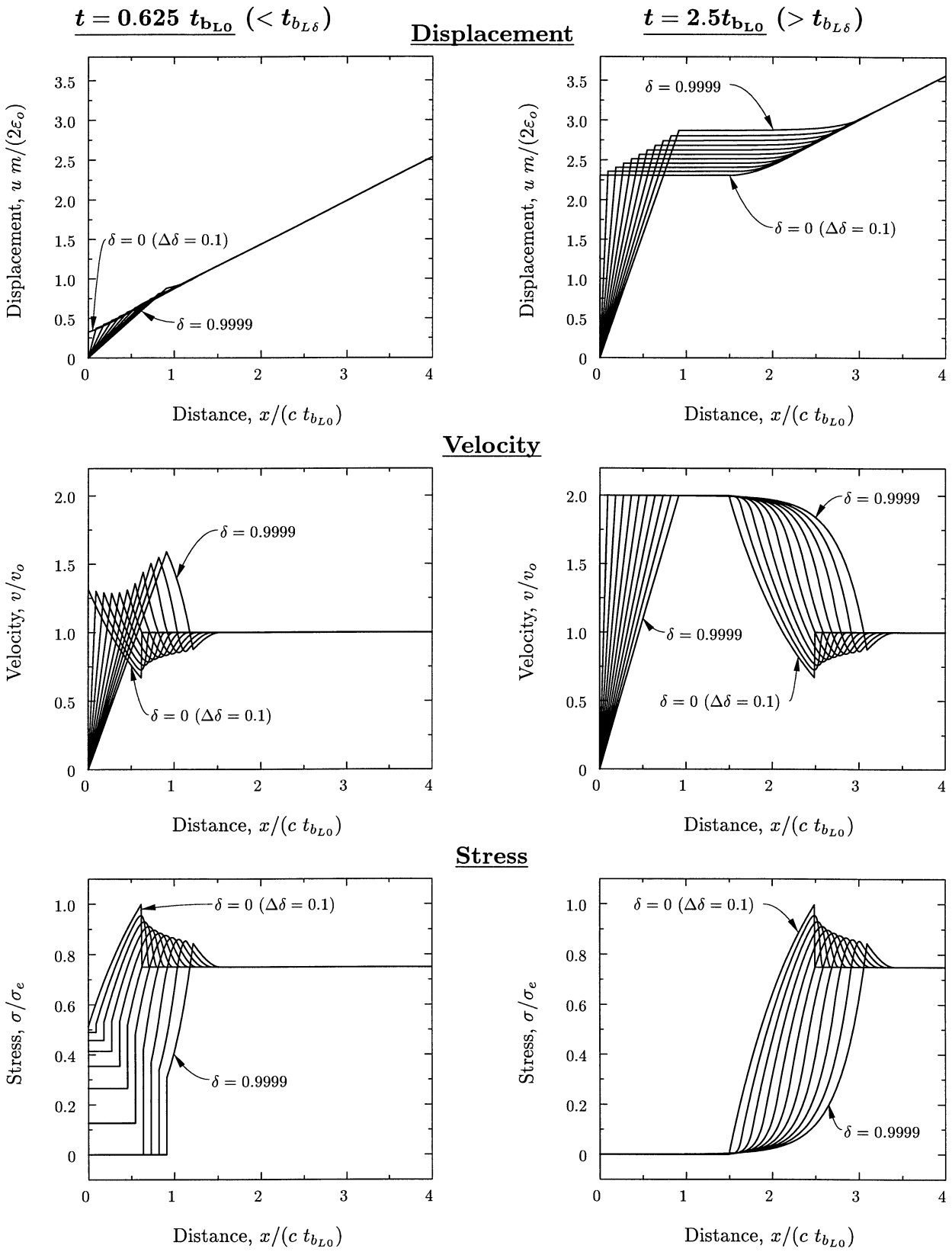

FIGURE 4.1. Displacement, velocity and stress distributions along the bar for $\delta = 0$, 0.1, 0.2, 0.3, 0.4, 0.5, 0.6, 0.7, 0.8, 0.9, and 0.9999, and at two given times: $t/t_{b_{L0}} = 0.625$ $(t < t_{b_{L\delta}})$ left column, and $t/t_{b_{L0}} = 2.5$ $(t > t_{b_{L\delta}})$ right column. Here, $t_{b_{L0}}$ is the breaking time for $\delta = 0$ given by (3.28), and $t_{b_{L\delta}}$ is the breaking time for the corresponding δ parameter.

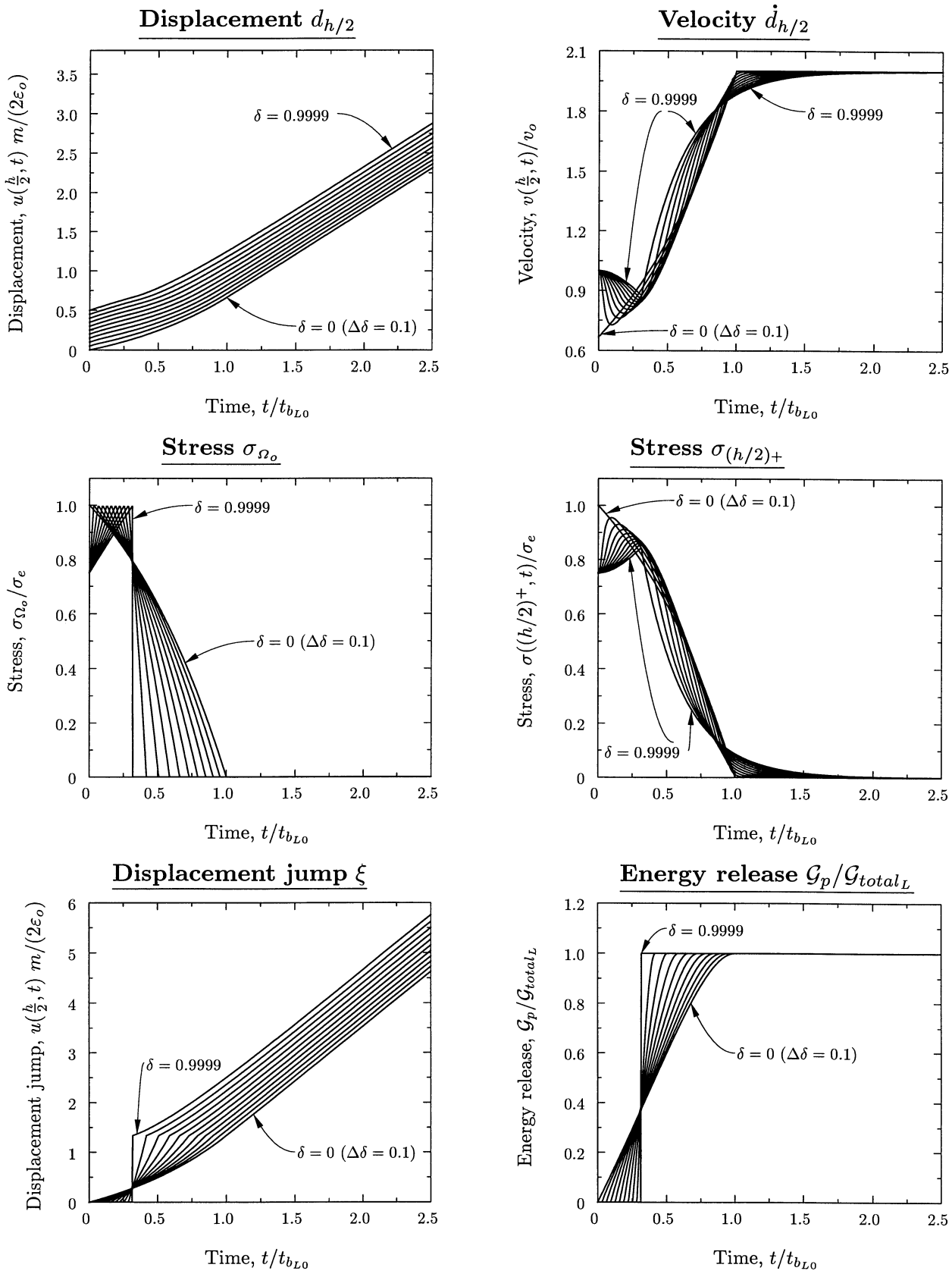

FIGURE 4.2. Displacement $d_{h/2}$, velocity $\dot{d}_{h/2}$, stress σ_{Ω_o}, stress $\sigma_{(h/2)+}$, displacement jump ξ, and energy release $\mathcal{G}_p/\mathcal{G}_{total_L}$ versus time for $\delta = 0$, 0.1, 0.2, 0.3, 0.4, 0.5, 0.6, 0.7, 0.8, 0.9, and 0.9999. The reference value $t_{b_{L0}}$ is the breaking time for $\delta = 0$ given by (3.28).

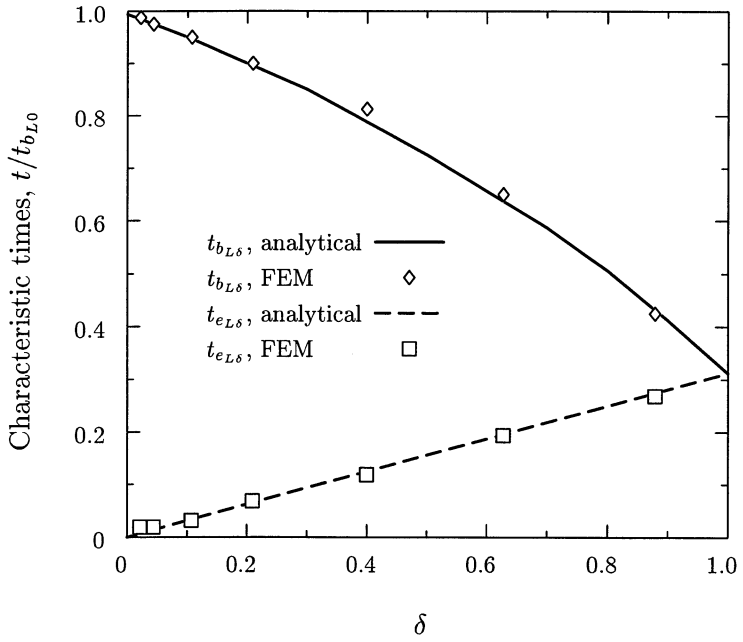

FIGURE 4.3. Yielding $t_{e_{L\delta}}$ and $t_{e_{L\delta}}$ breaking times for the linear softening law versus the non-dimensional parameter δ. The normalization parameter $t_{b_{L0}}$ is the breaking time for $\delta = 0$ given by (3.28).

The solution for the limit case $\delta = 0$ is also included in Figures 4.1 and 4.2. This case corresponds to the exact solution described in the previous section. The first difference that we can observe between the solutions with $\delta > 0$ and this limit solution is the presence of an initial time interval $t_{e_{L\delta}}$ during which the response of the bar, including the center $x = 0$, is elastic. This leads to a gradual variation of the stress in Ω_o from the initial value σ_o to the elastic limit σ_e. The "yielding time" $t_{e_{L\delta}}$ is depicted in Figure 4.3 as a function of the length parameter δ. We verify the increase of this time with δ.

The main consequence of the existence of this initial elastic phase is the absence of a propagating discontinuous loading front in the spatial distributions of the stress and velocity, as it occurs in the limit solution for $\delta = 0$. Instead, a smooth wave profile propagates along the bar, with a maximum stress value smaller that the elastic limit σ_e, the value associated to the front for $\delta = 0$. This feature can be explained as follows.

We first note the discontinuity of the stress at the fixed point $x = h/2$. This is due to the equivalent concentrated mass $\rho\vartheta h/2$ at $x = h/2$, with the corresponding acceleration, introduced by the assumed interpolation of the displacement; see equation (4.17). The constant approximation of σ_{Ω_o} in Ω_o can be observed in Figure 4.1. No smoothing of the stress distribution has been used in the plots. A negative acceleration $\ddot{d}_{h/2} \leq 0$ is to be expected in this initial elastic phase, since it corresponds to the decrease of the velocity

$\dot{d}_{h/2}$ characteristic of the loading that is occurring in Ω_o. Compare this situation with the elastic solution depicted in Figure 3.1. This negative acceleration can be verified in the graph of the velocity in Figure 4.2. As a consequence, the value of the stress $\sigma_{(h/2)+}$ outside Ω_o is smaller than the value of the stress σ_{Ω_o} in Ω_o, as concluded from equation (4.17). Therefore, the stress σ_{Ω_o} in Ω_o reaches the elastic limit σ_e before the stress outside Ω_o. This value is propagated elastically along the bar and, therefore, with a value smaller than σ_e. The resulting profile that propagates in the bar falls then below the limit case $\delta = 0$ in the magnitude of the stress. The corresponding value of the velocity is consequently higher than the value $(3.35)_1$ associated to the front for $\delta = 0$. In summary, the loading in this initial elastic phase occurs in a longer time interval as δ increases, but one can say that the loading in the bar outside Ω_o reaches a lower level.

Another curious feature of the solution for $\delta > 0$ is the fact that the propagating profile travels ahead of the discontinuous front corresponding to the limit case $\delta = 0$. See Figure 4.2. We recall that this front propagates at a speed c. Therefore, it may appear like signals propagate at a higher velocity for the case $\delta > 0$. Obviously, all signals in the elastic bar propagate at the constant wave speed c. Note that neither the profiles, nor the difference between profiles, become distorted during propagation, due to the absence of dispersive effects in the elastic bar. A careful observation reveals that the profile propagating ahead is due to the assumed interpolation in the finite width of Ω_o. In the finite length $h/2$, stress signals propagate instantaneously, as a consequence of the assumed interpolation $(4.1)_1$, defining the displacements and corresponding stress instantaneously everywhere in Ω_o in terms of the parameter $d_{h/2}$. Therefore, since a finite time is required for the front in the limit solution $\delta = 0$ to transverse the distance $h/2$, the propagating profile for $\delta > 0$ will be ahead. This explanation is confirmed by the plot of the velocity distribution in Figure 4.1 for $t = 2.5\ t_{b_{L0}}$. Note that the width of Ω_o, as it can be estimated from the linear variation at $x = 0$, corresponds to the distance between the discontinuous front and the tip of the propagating profile for $\delta > 0$. We emphasize that this feature is not associated to the presence of softening, like a change of type of the equations to elliptic, since we are still in the elastic range. The same effect will occur in a fully elastic solution, and it is purely an artifact of the assumed interpolation in the approximate solution.

Upon activation at $t_{e_{s\delta}}$ of the localized softening mechanism on the discontinuity at $x = 0$, the stress σ_{Ω_o} in Ω_o softens gradually. This decrease of the stress in Ω_o (on the left of $x = h/2$) leads to an increase of the acceleration $\ddot{d}_{h/2}$ from the previous elastic negative value in the initial elastic phase. Note here that the convention defines a positive displacement $d_{h/2}$ pointing to the right. The velocity $\dot{d}_{h/2}$ eventually reaches a minimum value, and starts increasing afterwards as shown in Figure 4.2. The stress $\sigma_{(h/2)+}$ outside Ω_o follows with elastic unloading. However, the positive acceleration indicates that the the stress $\sigma_{(h/2)+}$ is now higher that the stress in Ω_o. This can be verified in stress distribution shown in Figure 4.1 for $t = 0.625\ t_{b_{L0}} < t_{b_{L\delta}}$. This difference increases with the length parameter δ at a fixed time. This difference decreases, however, in time for a

TABLE 4.1. Problem definition. Material and geometric parameters.

Young modulus	E	$2 \cdot 10^4$
Density	ρ	$4 \cdot 10^{-8}$
Elastic limit	σ_e	$2 \cdot 10^0$
Localized softening modulus	$\tilde{\mathcal{H}}_L$	$-4 \cdot 10^{-2}$
Length	L	$4\ c\ t_{b_{L0}}$
Initial conditions	r	1.5

fixed parameter δ, especially after the stress σ_{Ω_o} in Ω_o vanishes (i.e., breaking), as discussed below.

This situation identifies a faster release of the stress in Ω_o as δ increases. This feature can be observed explicitly in the evolution of σ_{Ω_o} in time depicted in Figure 4.2. Surprisingly, even though the time required to activate the softening response $t_{e_{L\delta}}$ is larger for a larger δ, the final breaking time $t_{b_{L\delta}}$ is smaller. This is shown in Figure 4.3, depicting both characteristic times as a function of the length parameter δ. As a consequence, the time interval during which the softening response takes place reduces with the width approximating the localized effects. The more brittle response of the discretized bar as δ increases follows. This feature is to be expected given the more negative value of the regularized tangent modulus in $(4.12)_2$. In fact, in the limit $\delta \to 1$, the stress is released instantaneously. We note, however, that the dissipated energy is still finite, as shown in Figure 4.2. The reason is that this sudden release of the stress is accompanied by a sudden change of the displacement jump on the discontinuity inside Ω_o. The displacement jump becomes discontinuous in time, that is, the bar breaks suddenly, a limit brittle response.

After breaking at $t_{b_{s\delta}}$, the velocity $\dot{d}_{h/2}$ and the stress $\sigma_{(h/2)+}$ at $x = h/2^+$ gradually evolve to their limit values $2v_o$ and 0, respectively, as in the exact solution for $\delta = 0$. This can be observed in the time plots of Figure 4.2. In fact, according to (4.28), and given the expression (4.19) for the stress at $x = h/2^+$, these limit values are approached exponentially at a rate given by the parameter γ defined in (4.29). All the different properties of the solution described above lead to a final profile propagating along the elastic bar that can be considered as a smooth approximation of the exact solution given by the limit case $\delta = 0$, its large-scale regularization.

4.2. Representative finite element simulations

To validate the extrapolation of the above conclusions to actual finite element simulations of the full boundary value problem, we present in this section the results obtained for several representative simulations. We consider the bar $\Omega = [-L, L]$ discretized symmetrically by an odd number of equal length linear finite elements. The treatment of the

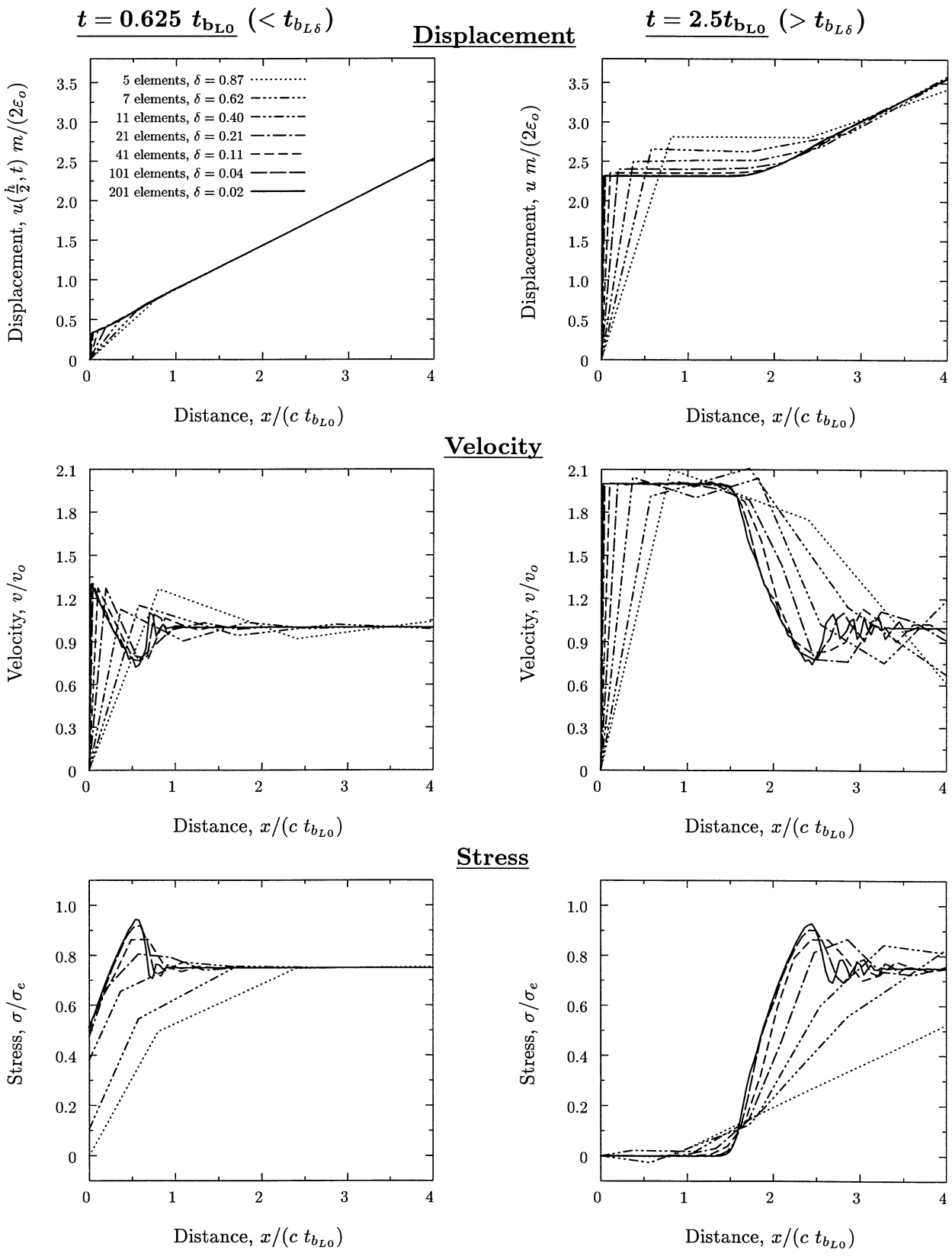

FIGURE 4.4. Finite element solution. Displacement, velocity and stress distributions along the bar for different number of elements and at two given times: $t/t_{b_{L0}} = 0.625$ $(t < t_{b_{L\delta}})$ left column, and $t/t_{b_{L0}} = 2.5$ $(t > t_{b_{L\delta}})$ right column. All plots follow the same legend as in the top left figure.

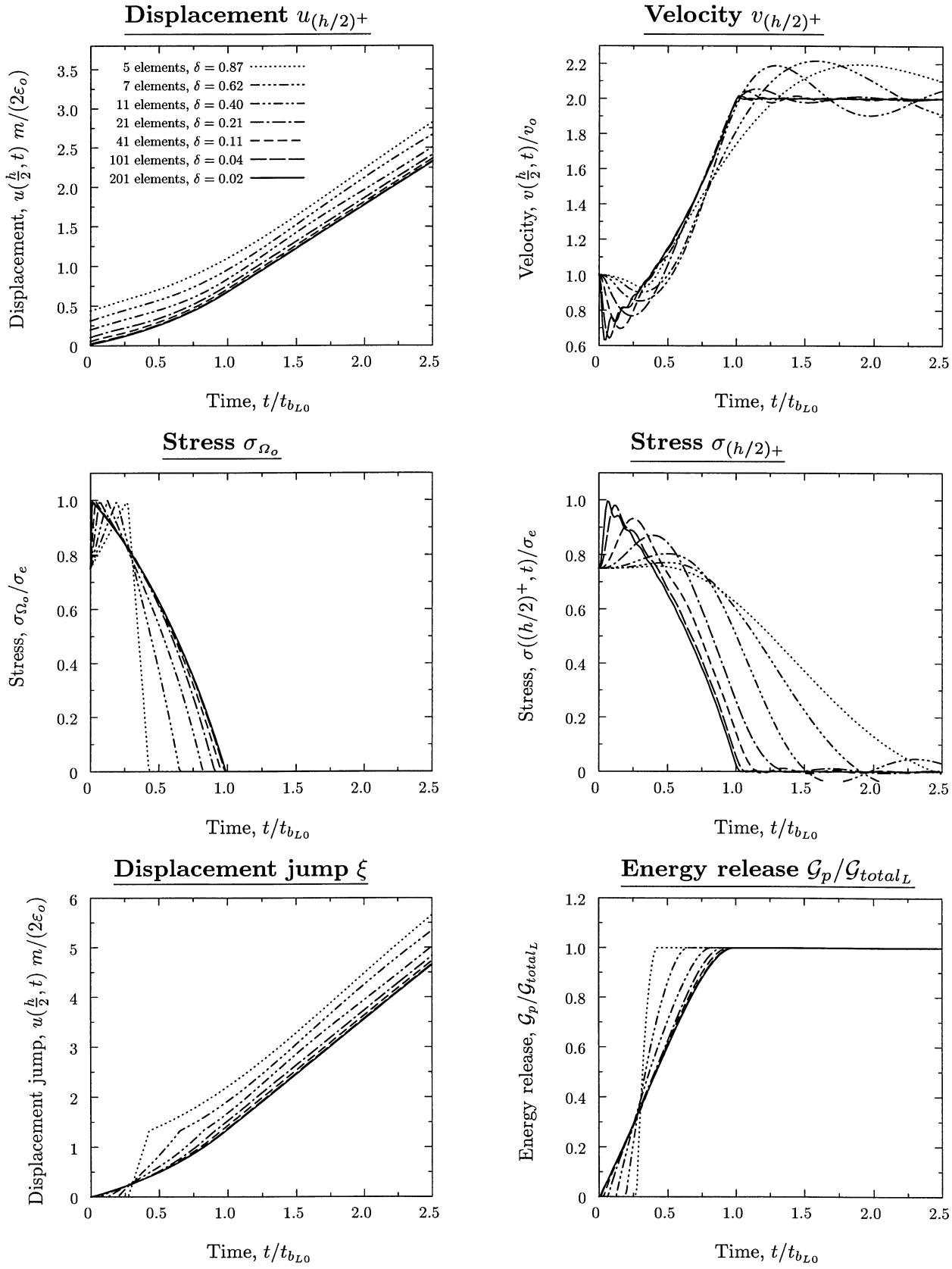

FIGURE 4.5. Displacement $u_{(h/2)+}$, velocity $v_{(h/2)+}$, stress σ_{Ω_o}, stress $\sigma_{(h/2)+}$, displacement jump ξ, and energy release $\mathcal{G}_p/\mathcal{G}_{total_L}$ obtained with finite elements. All plots follow the same legend as in the top left figure.

constitutive relations in the central element follows exactly the discussion presented in the previous section. Outside this central element the response is confirmed to be linear elastic as in the analytical solution obtained before.

The initial conditions (3.3) are considered at $t = 0$, with an initial constant velocity v_o. A stress of $r = 1.5$ (i.e., $\sigma_o = 0.75\ \sigma_e$) is imposed at the ends of the bar as in the previous discussion. For completeness, we summarize in Table 4.2 the material and geometric properties assumed in the simulations. Given the scaling of the different quantities when depicting the results, the solutions reported herein are, however, independent of the actual values of these material parameters. We consider the average acceleration Newmark approximation ($\beta = 1/4$, $\gamma = 1/2$) of the governing equations in time, with a consistent mass matrix and a constant time step of $\Delta t = t_{b_{L0}}/80$ for all the simulations. Our goal is to study the effects of the spatial discretization in the final solution and, in particular, validate the conclusions drawn above from the analytical solutions. Alternative temporal approximations and/or non-uniform spatial discretizations are not considered for the sake of brevity.

Figures 4.4 and 4.5 depict the results obtained with different number of elements. Only one half of the bar is depicted (and, in fact, computed by considering half of the central element), by symmetry. The reported number of elements, however, indicates again the number of equal elements for the full bar of length $2L$. The corresponding non-dimensional length parameter δ is also reported in these figures, and it ranges from 0.87 to 0.002. As it is customary in finite element analyses, the reported stress distributions in Figure 4.4 are obtained by projecting the element values to the nodes. The time evolution of the stresses σ_{Ω_o} and $\sigma_{\frac{h}{2}+}$ in Figure 4.5 correspond, instead, to the computed values in the central and adjacent element, respectively.

Comparing the finite element solutions with the analytical solutions in Figures 4.1 and 4.2, we can observe a very good agreement. In fact, the conclusions drawn in the previous section from the study of the analytical solutions can be confirmed in these fully discrete results, although with the difficulty of considering the pollution added to the numerical solutions by the discretization of the elastic part of the bar. In particular, the smoothing of the front present in the limit solution $\delta = 0$ with increasing δ can be clearly verified. All quantities correlate well. In particular, we have included in Figure 4.3 the yielding and breaking times estimated in the finite element simulations. The good agreement with the analytical curves (obtained by solving $(4.21)_2$ and $(4.24)_2$, respectively) is to be noted. We conclude that the analysis presented in Section 4.1 gives a good understanding of the properties of discrete approximations of the singular fields associated to strong discontinuities in this general dynamic setting.

5. Concluding Remarks

The developments presented in this paper identify a general framework for the incorporation of localized dissipative effects in the large-scale problem of the local continuum. In particular, we have shown that the local consideration of strong discontinuities leads to an efficient tool for the modeling of localized dissipative mechanisms characteristic of localized failures of inelastic solids. We have presented briefly the examples of localized elastoplastic and damage responses, both formulated in the thermodynamic framework furnished by the principle of maximum inelastic dissipation.

It is important to emphasize that the characterization of these localized mechanisms is accomplished in the small scale without the need of introducing any type of smearing. nor any type of artificial length parameters. Still, this characterization is done in a local neighborhood of the material points. It is the bridge between the two problems, the large-scale balance equations and the local constitutive equations, that identifies the proper length scales present in the problem. In particular, we have shown that equating the dissipation of the two problems leads to a consistent formulation in the limit of the local continuum, involving no artificial length scale parameters in this limit, and incorporating by construction the dissipative effects of the material in the large-scale problem of interest. The resulting *localized models* are then mechanically sound.

Furthermore, the constructive procedure employed in these developments identifies the framework of what we refer to as *large-scale regularizations* of the problem. These regularizations are characterized by a smooth large-scale displacement, with the local singular fields associated to the strong discontinuity available at the finite local neighborhood through the bridge equation. They should not be confused with the so-called regularized strong discontinuity approaches, consisting of a finite band even at the local level. We note in this respect the importance that the focus on the limit problem involving discontinuous solutions has in these considerations. We believe that these ideas identify an interesting framework for the understanding of related existing techniques like, for example, techniques based on the traditional smeared assumption. Moreover, although it has not been investigated in this paper, the generality gained by the proposed approach leads, in particular, to alternative finite element techniques for the solution of these problems, as we have presented in our previous work in this area.

Instead, we have directed our attention in this paper to the analysis of wave propagation in an softening bar. The focus on the limit case of a discontinuous solution incorporating the localized response of the material has proven again to be very useful for a complete understanding of the problem. In particular, it allows to obtain the exact closed-form solution for a general cohesive softening law on the discontinuity. The final solution shows to be physically meaningful, in contrast with the non-physical solution obtained for a continuum strain-softening material model. The finite amount of energy dissipation and the continuous dependence on the model parameters, as expected from physical considerations,

are present in the solution.

The consideration of a discrete large-scale regularization of the problem and its analytical solution has revealed several approximation properties of commonly used discretization techniques for the solution of these problems. This analysis also furnishes the exact closed-form solution for the case of a regularized discontinuity, involving a band of constant width. In the context of the one-dimensional dynamical problem under study, we have identified the addition of a transient term in the softening response of the material when a finite discrete length is assumed to represent the localized softening effects. The main consequence of this approximation can be summarized as the smoothing of the propagating fronts that appear in the solution, accompanied with the expected more brittle response of the discrete solid. These conclusions have been verified in actual finite element simulations of the problem.

Acknowledgments

Financial support for this research has been provided by the ONR under contract no. N00014-96-1-0818 and the NSF under contract no. CMS-9703000 with UC Berkeley. This support is gratefully acknowledged.

References

ARMERO, F. [1997a] "Large-Scale Modeling of Localized Dissipative Mechanisms in a Local Continuum: Applications to the Numerical Simulation of Strain Localization in Rate-Dependent Inelastic Solids," SEMM/UCB Report no. 97/12, submitted to *Mech. Cohesive-Frictional Mat.*

ARMERO, F. & GARIKIPATI, K. [1995] "Recent Advances in the Analysis and Numerical Simulation of Strain Localization in Inelastic Solids," *Proc. COMPLAS IV,* eds. D.R.J. Owen, E. Onate, and E. Hinton, CIMNE, Barcelona.

ARMERO, F. & GARIKIPATI, K. [1996] "An Analysis of Strong Discontinuities in Multiplicative Finite Strain Plasticity and their Relation with the Numerical Simulation of Strain Localization in Solids," *Int. J. Solids and Structures,* **33**, 2863-2885.

BAI, Y. & DODD, B. [1992] *Adiabatic Shear Localization; Occurrence, Theories and Localization,* Pergamon Press, Oxford.

BAZANT, Z.P.; BELYTSCHKO, M. & CHANG, T.P. [1984] "Continuum Theory for Strain-Softening", *J. Eng. Mech., ASCE,* **110**, 1666-1691.

BAZANT, Z. & BELYTSCHKO, T. [1985] "Wave Propagation in a Strain Softening Bar," *ASCE J. Eng. Mech.,* **111**, 381-389.

BAZANT & OH [1983] "Crack Band Theory for Fracture of Concrete," *Materials and Structures,* RILEM, **16**, 155-177.

BELYRSCHKO, T.; FISH, J. & ENGELMANN, B.E. [1988] "A Finite Element with Embedded Localization Zones," *Comp. Meth. Appl. Mech. Eng.,* **70**, 59-89.

DEBORST, R. & SLUYS, L.J. [1991] "Localization in a Cosserat Continuum under Static and Loading Conditions", *Comp. Meth. Appl. Mech. Eng.,* **90**, 805-827.

COLEMAN, B.D. & HODGON, M.L. [1985] "On Shear Bands in Ductile Materials", *Arch. Rat. Mech. Analy.,* **90**, 219-247.

DVORKIN, E.; CUITIÑO, A. & GOIA, G. [1990] "Finite Elements with Displacement Interpolated Embedded Localization Lines Insensitive to Mesh and Distortions," *Int. J. Num. Meth. Eng.,* **30**, 541-564.

HILL, R. [1950] *The Mathematical Theory of Plasticity,* Clarendon Press, Oxford.

HILL, R. [1962] "Acceleration Waves in Solids," *J. Mech. Phys. Solids,* **16**, 1-10.

HUGHES, T.J.R. [1996] "Multiscale Phenomena: Green's Function, the Dirichlet-to-Neumann Formulation, Subgrid Scale Models, Bubbles and the Origin of the Stabilized Methods," *Computer Methods in Applied Mechanics and Engineering,* **127**, 387-401.

JOHNSON, C. [1976] "Existence Theorems for Plasticity Problems," *J. Math. Pures et Appliq.* **55**, 431-444.

LARSSON, R. & RUNESSON, K. [1996] "Element Embedded Localization Band Based on Regularized Displacement Discontinuity", *J. Eng. Mech.,* **122**, 402-411.

MANDEL, J. [1966] "Conditions de Stabilité et Postulat de Drucker", in *Rheology and Soli Mechanics,* IUTAM Symposium, Grenoble 1964, ed. by J. Kravtchenko and P.M. Sirieys, 58-68.

MATTHIES, H.; STRANG, G. & CHRISTIANSEN, E. [1979] "The Saddle Point of a Differential Program," in *Energy Methods in Finite Element Analyses,* edited by Glowinski, Rodin & Zienkiewicz, John Wiley & Sons, London.

MOLINARI, A. & CLIFTON, R.J. [1987] "Analytical Characterization of Shear Localization in Thermoviscoplastic Materials," *Journal of Applied Mechanics,* **54**, 806-812.

NEEDLEMAN, A. [1988] "Material Rate Dependence and Mesh Sensitivity in Localization Problems," *Comp. Meth. Appl. Mech. Eng.*, **67**, 69-85.

NEILSEN, M.K. & SCHREYER, H.L. [1993] "Bifurcation in Elastic-Plastic Materials," *Int. J. Solids Struct.,* **30**, 521-544.

OLIVER, J. [1989] "A Consistent Characteristic Length for Smeared Cracking Problems", *Int. J. Num. Meth. Eng.*, **28**, 461-474.

OLIVER, J. [1996] "Modelling Strong Discontinuities in Solid Mechanics via Strain Softening Constitutive Equations. Part 1: Fundamentals. Part 2: Numerical Simulation," *Int. J. Num. Meth. Eng.*, **39**, 3575-3623.

ORTIZ, M. [1985] "A Constitutive Theory for the Inelastic Behavior of Concrete," *Mech. Mat.*, **4**, 67-93.

ORTIZ, M.; LEROY, Y. & NEEDLEMAN, A. [1987] "A Finite Element Method for Localized Failure Analysis," *Comp. Meth. Appl. Mech. Eng.*, **61**, 189-214.

OTTOSEN, N.S. & RUNESSON, K. [1991] "Properties of Discontinuous Bifurcation Solutions in Elasto-Plasticity," *Int. J. Solids Struct.*, **27**, 401-421.

PIETRSZCZAK, ST. & MRÓZ, Z. [1981] "Finite Element Analysis of Deformation of Strain-Softening Materials," *Int. J. Numer. Meth. Eng.*, **17**, 327-334.

PRANDTL, L. [1920] "Ueber die Haerte Plastischer Koerper," *Goettinger Nachrichten,* 74-84.

READ, H.E. & HEGEMEIER, G.A. [1984] "Strain Softening of Rock, Soil and Concrete; a Review Article," *Mechanics of Materials,* **3**, 271-294.

RICE, J. [1976] "The Localization of Plastic Deformations", in *Theoretical and Applied Mechanics,* ed. by W.T. Koiter, 207-219.

ROTS, J.G.; NAUTA, P.; KUSTERS, G. & BLAAUWENDRAA, T. [1985] "Smeared Crack Approach and Fracture Localization in Concrete," *Heron,* **30**.

SIMO, J.C; OLIVER, J. & ARMERO, F. [1993] "An Analysis of Strong Discontinuities Induced by Softening Solutions in Rate Independent Solids," *J. Comput. Mech.*, **12**, 277-296.

SIMO, J.C. & RIFAI, S. [1990] "A Class of Mixed Assumed Strain Methods and the Method of Incompatible Modes," *Int. J. Num. Meth. Eng.*, **29**, 1595-1638.

STAKGOLD, I. [1979] *Green's Functions and Boundary Value Problems,* Wiley, New York.

SUQUET, P.M. [1981] "Sur les Equations de la Plasticité: Existence et Régularité des Solutions," *Journal de Mécannique,* **20**, 3-39.

STEINMANN, P.; LARSSON, R. & RUNESSON, K. "On the Localization Properties of Multiplicative Hyperelasto-plastic Continua with Strong Discontinuities," *Int. Jour. Solids Structures,* **34**, 969-990.

TEMAM, R. [1984] *Mathematical Problems in Plasticity,* Gauthier-Villars, Paris.

THOMAS, T.Y. [1961] *Plastic Flow and Fracture in Solids,* Academic Press.

TRUESDELL & NOLL [1965] "The Nonlinear Field Theories of Mechanics," *Handbich der Physik Bd. III/3,* ed. by S. Fluegge, Springer Verlag, Berlin.

VARDOULAKIS, I. [1979] "Formataion of Shear Bands in Sand Bodies as a Bifurcation Problem," *Int. J. ,* **32**, 35-54.

WILLAM, K.; BICANIC, N. & STURE, S. [1984] "Constitutive and Computational Aspects of Strain Softening and Localization in Solids," *ASME/WAM 1984 Symp. on Constitutive Equations: Macro and Computational Aspects,* ed. by K. Willam, ASME, New York, 233-252.

WILLAM, K.; PRAMONO, E. & STURE, S. [1986] "Stability and Uniqueness of Strain-Softening Computation," *Europe-US Symp. on Finite Elem. Meth. Nonlinear Probl.,* ed. by P. Bergan, W. Wunderlich and K.J. Bathe, Springer Verlag, Berlin, 119-142.